

SUPPLEMENTARY INFORMATION

Tbx16 regulates *hox* gene activation in mesodermal progenitor cells

Alexander Y. Payumo[†], Lindsey E. McQuade^{†,§}, Whitney J. Walker[†]

Sayumi Yamazoe[†], and James K. Chen^{*,†,‡},

[†]Department of Chemical and Systems Biology, Stanford University School of Medicine, Stanford, CA 94305, USA

[‡]Department of Developmental Biology, Stanford University School of Medicine, Stanford, CA 94305, USA

[§]Present address: Department of Chemistry, University of Illinois, Chicago, IL 60607, USA

*Corresponding author. Department of Chemical and Systems Biology, Stanford University School of Medicine, 269 Campus Drive, CCSR 3155, Stanford, CA 94305, USA. Tel: 650-725-3582. Fax: 650-723-2253. Email: jameschen@stanford.edu.

SUPPLEMENTARY RESULTS

Supplementary Table 1	3-5
Supplementary Table 2	6-8
Supplementary Table 3	9-11
Supplementary Figure 1	12
Supplementary Figure 2	13
Supplementary Figure 3	14
Supplementary Figure 4	15
Supplementary Figure 5	16
Supplementary Figure 6	17
Supplementary Figure 7	18
Supplementary Figure 8	19
Supplementary Figure 9	20
Supplementary Figure 10	21
Supplementary Figure 11	22
Supplementary Figure 12	23
Supplementary Figure 13	24
Supplementary Figure 14	25
Supplementary Figure 15	26
Supplementary Figure 16	27
Supplementary Movies 1-3	28-29
References	30-35

Supplementary Table 1. cFD vs. *tbx16* cMO + cFD comparison at 9 hpf: 64 downregulated genes ranked by fold-change

Sequences were aligned to zebrafish genome assembly Zv8. False-discovery rate < 0.01.

*Confirmation by whole-mount *in situ* hybridization

Entry	RefSeqID	Gene symbol	Gene description	Fold change	Expression pattern during gastrulation and somitogenesis	Embryonic function	Functional annotation in IPA	Previously known Tbx16 target?	Validated in this study?*
1	NM_214786	<i>asic4b</i>	acid sensing (proton-gated) ion channel family member 4b	-19.83					
2	NM_001204257	<i>ppp1r13ba</i>	protein phosphatase 1, regulatory subunit 13Ba	-7.17	ventral anterior mesoderm ¹				
3	NM_182885	<i>pcdh10b</i>	protocadherin 10b	-4.80	paraxial mesoderm	somitogenesis ²		Yes ^{3,4}	Yes
4	NM_001166446	<i>si:dkey-261j4.4</i>	si:dkey-261j4.4	-4.48					
5	NR_030084	<i>mir133b</i>	microRNA 133b	-4.45		myogenesis ⁵			
6	NM_001039109	<i>rippy2</i>	rippy2	-4.17	paraxial mesoderm	somitogenesis ⁶			Yes
7	NM_131209	<i>pcdh8</i>	protocadherin 8	-4.17	ventrolateral margin ⁷	gastrulation movements ⁸		Yes ^{3,4}	
8	NM_001166445	<i>si:dkey-261j4.3</i>	si:dkey-261j4.3	-3.80					
9	NM_130972	<i>tcf15</i>	transcription factor 15 (basic helix-loop-helix)	-3.68	paraxial mesoderm ⁹		AP patterning, myogenesis, somitogenesis		
10	NM_001003886	<i>her11</i>	hairy-related 11	-3.56	paraxial mesoderm	somitogenesis ¹⁰			Yes
11	NM_001113337	<i>cyp27c1</i>	cytochrome P450, family 27, subfamily C, polypeptide 1	-3.39	margin ¹¹				
12	NM_173227	<i>sebox</i>	SEBOX homeobox	-3.12	margin ¹²				
13	NM_200965	<i>atp2a2a</i>	ATPase, Ca++ transporting, cardiac muscle, slow twitch 2a	-3.09	paraxial mesoderm, tailbud				Yes
14	NM_212733	<i>tpd52l2a</i>	tumor protein D52-like 2a	-3.05	unspecified ¹³				
15	NM_001082947	<i>nr0b1</i>	nuclear receptor subfamily 0, group B, member 1	-2.99	ubiquitous ¹⁴				
16	NM_182882	<i>msgn1</i>	mesogenin 1	-2.96	tailbud	somitogenesis ^{15,16}	myogenesis, somitogenesis	Yes ^{3,4}	Yes
17	NM_001110166	<i>calcoco1a</i>	calcium binding and coiled-coil domain 1a	-2.64					
18	NM_213274	<i>cldn5a</i>	claudin 5a	-2.62	axial mesoderm, tailbud ¹³				
19	NM_153650	<i>has2</i>	hyaluronan synthase 2	-2.55	ventrolateral margin ⁹	gastrulation movements ¹⁷	myogenesis, epithelial-mesenchymal transition		
20	NM_001080012	<i>hhip</i>	hedgehog interacting protein	-2.51	adaxial, lateral mesoderm ¹⁸	myogenesis ¹⁸			
21	NM_178307	<i>cxcl12a</i>	chemokine (C-X-C motif) ligand 12a (stromal cell-derived factor 1)	-2.51	paraxial mesoderm	myogenesis ¹⁹			Yes
22	NM_131037	<i>fsta</i>	follistatin a	-2.43	paraxial mesoderm		myogenesis		Yes
23	NM_001033727	<i>draxin</i>	dorsal inhibitor axon guidance protein	-2.38	paraxial mesoderm ²⁰				
24	NM_200860	<i>arl4aa</i>	ADP-ribosylation factor-like 4aa	-2.34	axial, paraxial mesoderm ¹³				
25	NM_213153	<i>dnase1l3</i>	deoxyribonuclease 1-like 3	-2.11	Kupffer's vesicle ¹³				
26	NM_173283	<i>igfbp1a</i>	insulin-like growth factor binding protein 1a	-2.11	adaxial mesoderm ¹				
27	NM_198911	<i>sept9a</i>	septin 9a	-2.08	axial, ventral				

					mesoderm ¹				
28	NM_001001409	<i>actc1a</i>	actin, alpha, cardiac muscle 1a	-2.07	adaxial mesoderm		myogenesis		Yes
29	NM_001098388	<i>zcchc24</i>	zinc finger, CCHC domain containing 24	-2.06					
30	NM_205585	<i>sfrp1a</i>	secreted frizzled-related protein 1a	-2.03	paraxial mesoderm ²¹		AP patterning, somitogenesis		
31	NM_001002366	<i>tjp2b</i>	tight junction protein 2b (zona occludens 2)	-1.98	paraxial mesoderm ¹³				
32	NM_131728	<i>foxc1a</i>	forkhead box C1a	-1.96	paraxial mesoderm ¹³	somitogenesis ²²	myogenesis	Yes ²²	
33	NM_201174	<i>rem1</i>	RAS (RAD and GEM)-like GTP-binding 1	-1.93	paraxial mesoderm, tailbud				Yes
34	NM_001003532	<i>desi2</i>	desumoylating isopeptidase 2	-1.93	dorsalventral margin ¹	gastrulation movements ²³			
35	NM_131233	<i>gata2a</i>	GATA binding protein 2a	-1.89	ventral region ²⁴				
36	NM_131850	<i>aldh1a2</i>	aldehyde dehydrogenase 1	-1.87	paraxial mesoderm ²⁵	AP patterning ²⁶	AP patterning, myogenesis, somitogenesis	Yes ⁴	
37	NM_131729	<i>foxc1b</i>	forkhead box C1b	-1.86	adaxial, paraxial mesoderm		myogenesis		Yes
38	NM_001115094	<i>notch2</i>	notch homolog 2	-1.86	axial, paraxial mesoderm		epithelial- mesenchymal transition		Yes
39	NM_001013521	<i>enah</i>	enabled homolog (Drosophila)	-1.84	paraxial mesoderm ²⁷				
40	NM_130917	<i>fzd10</i>	frizzled class receptor 10	-1.84	tailbud				
41	NM_131269	<i>tcf7l1a</i>	transcription factor 7-like 1a	-1.80	axial, paraxial mesoderm ¹³				
42	NM_001013555	<i>aoc2</i>	amine oxidase, copper containing 2	-1.79					
43	NM_130960	<i>lft1</i>	lefty1	-1.79	axial mesoderm, margin ¹	gastrulation movements ²⁸			
44	NM_131052	<i>tbx6l</i>	T-box 6, like	-1.78	paraxial mesoderm, tailbud			Yes ^{3,4}	Yes
45	NM_001265583	<i>mespab</i>	mesoderm posterior ab	-1.74	paraxial mesoderm				Yes
46	NM_001002389	<i>ip6k2b</i>	inositol hexakisphosphate kinase 2b	-1.74	axial mesoderm ¹³				
47	NM_182871	<i>fgf24</i>	fibroblast growth factor 24	-1.74	margin, prechordal plate ⁹	AP patterning ²⁹		Yes ²⁹	
48	NM_001007063	<i>magi1b</i>	membrane associated guanylate kinase, WW and PDZ domain containing 1b	-1.73					
49	NM_001042746	<i>tshz1</i>	teashirt zinc finger	-1.71	neural tube ³⁰		AP patterning		
50	NM_131893	<i>meis1b</i>	Meis homeobox 1 b	-1.71	paraxial mesoderm				
51	NM_213495	<i>cul1b</i>	cullin 1b	-1.71	unspecified ¹³				
52	NM_199429	<i>pigg</i>	phosphatidylinositol glycan anchor biosynthesis, class Q	-1.68	ventral mesoderm ¹				
53	NM_001075105	<i>aplnra</i>	apelin receptor a	-1.67	adaxial mesoderm	gastrulation movements ³¹			Yes
54	NM_213248	<i>arl4cb</i>	ADP-ribosylation factor-like 4Cb	-1.64	eye, neural tube ¹³				
55	NM_001013261	<i>fn1b</i>	fibronectin 1b	-1.62	paraxial mesoderm ¹³	somitogenesis ³²			
56	NM_001077794	<i>dact2</i>	dishevelled-binding antagonist of beta- catenin 2	-1.61	tailbud, notochord, intermediate mesoderm ³³				
57	NM_001006044	<i>cldn5b</i>	claudin 5b	-1.60	ventral mesoderm ¹³				
58	NM_199521	<i>siah1</i>	siah E3 ubiquitin protein ligase 1	-1.60	ventrolateral margin ²⁷				
59	NM_001030197	<i>aplnrb</i>	apelin receptor b	-1.57	adaxial mesoderm	gastrulation movements ³⁴			Yes
60	NM_131718	<i>six4a</i>	SIX homeobox 4a	-1.55	paraxial mesoderm ³⁵		myogenesis		

61	NM_001172683	<i>tcf3b</i>	transcription factor 3b	-1.55						
62	NM_131078	<i>her1</i>	hairy-related 1	-1.54	ventrolateral margin ⁹	somitogenesis ³⁶		Yes ^{3,4}		
63	NM_170763	<i>fzd7b</i>	frizzled class receptor 7b	-1.50	paraxial mesoderm	gastrulation movements ³⁷			Yes	
64	NM_131564	<i>appa</i>	amyloid beta (A4) precursor protein a	-1.50						

Supplementary Table 2. cFD vs. *tbx16* cMO + cFD comparison at 9 hpf: 60 upregulated genes ranked by fold-change

Sequences were aligned to zebrafish genome assembly Zv8. False-discovery rate < 0.01.

*Confirmation by whole-mount *in situ* hybridization

Entry	RefSeqID	Gene symbol	Gene description	Fold change	Expression pattern during gastrulation and somitogenesis	Embryonic function	Functional annotation in IPA	Previously known Tbx16 target?	Validated in this study?*
1	NM_214777	<i>b3gnt7l</i>	UDP-GlcNAc:betaGal beta-1,3-N-acetylglucosaminyltransferase 7, like	4.83					
2	NM_213184	<i>nfkbiaa</i>	nuclear factor of kappa light polypeptide gene enhancer in B-cells inhibitor, alpha a (nfkbiaa)	4.75	tailbud ¹³		myogenesis, epithelial-mesenchymal transition		
3	NM_001030164	<i>hivep2a</i>	human immunodeficiency virus type I enhancer bindingprotein 2a	4.58	paraxial mesoderm ⁹				Yes
4	NM_001014353	<i>alpi.1</i>	alkaline phosphatase, intestinal, tandem duplicate 1	4.27	adaxial mesoderm ¹³				
5	NM_001126448	<i>lect1</i>	leukocyte cell derived chemotaxin 1	4.26	axial mesoderm ¹				
6	NM_001128784	<i>sst6</i>	somatostatin 6	4.09					
7	NM_131290	<i>foxd3</i>	forkhead box D3	3.65	ubiquitous, dorsal ³⁸				
8	NM_131063	<i>shha</i>	sonice hedgehog a	3.62	axial mesoderm ³⁹	Myogenesis ³⁹	AP patterning, myogenesis		
9	NM_001012367	<i>mcamb</i>	melanoma cell adhesion molecule b	3.57	lateral mesoderm, tailbud ²⁷		epithelial-mesenchymal transition		
10	NM_131155	<i>hoxa10b</i>	homeobox A10b	3.17	tailbud	AP patterning ⁴⁰	AP patterning		Yes
11	NM_001089454	<i>zgc:162707</i>	<i>zgc:162707</i>	3.11					
12	NM_001002219	<i>htra1a</i>	HtrA serine peptidase	3.08	ubiquitous ¹³	AP patterning ⁴¹			
13	NM_001020514	<i>ncs1b</i>	neuronal calcium sensor 1b	2.85					
14	NM_001202417	<i>marveld1</i>	MARVEL domain containing 1	2.80	ubiquitous, higher in neural plate ¹³				
15	NM_131359	<i>bmp2a</i>	bone morphogenetic protein 2a	2.69	margin, tailbud		myogenesis, epithelial-mesenchymal transition		Yes
16	NM_131194	<i>hoxa13b</i>	homeobox A13b	2.67	tailbud	AP patterning, myogenesis ⁴⁰			Yes
17	NM_001029963	<i>ppp1r14c</i>	protein phosphatase 1, regulatory (inhibitor) subunit 14C	2.66					
18	NM_131691	<i>s1pr1</i>	sphingosine-1-phosphate receptor	2.62		gastrulation movements ⁴²			Yes
19	NM_131533	<i>hoxa9b</i>	homeobox A9b	2.54	tailbud	AP patterning ⁴⁰			Yes
20	NM_001100039	<i>arid3c</i>	AT rich interactive domain 3C (BRIGHT-like)	2.50					
21	NM_201332	<i>rab32a</i>	RAB32a, member RAS oncogene family	2.43	axial mesoderm ¹				
22	NM_001254944	<i>hoxc10a</i>	homeobox C10a	2.36	tailbud	AP patterning ⁴⁰	AP patterning		Yes
23	NM_199720	<i>tagln3b</i>	transgelin 3b	2.26	tailbud				Yes
24	NM_001099344	<i>kirrel3l</i>	kin of IRRE like 3 like	2.09	axial mesoderm	myogenesis ⁴³			
25	NM_199658	<i>insm1b</i>	insulinoma-associated 1b	2.04	neural tissue ⁴⁴				
26	NM_200637	<i>adam8a</i>	ADAM metallopeptidase domain 8a	2.03	tailbud				Yes
27	NM_001130818	<i>tspan7b</i>	tetraspanin 7b	2.02	axial mesoderm ¹³				

28	NM_200810	<i>ppp1r14ab</i>	protein phosphatase 1, regulatory (inhibitor) subunit 14Ab	2.02	ventral mesoderm, neural tissue ¹³	AP patterning ⁴⁵			
29	NM_001077282	<i>nedd9</i>	neural precursor cell expressed, developmentally down-regulated 9	2.01					
30	NM_205670	<i>tmem88a</i>	transmembrane protein 88 a	1.99	ventral mesoderm ¹³				
31	NM_001114437	<i>brinp3a</i>	bone morphogenetic protein/retinoic acid inducible neural-specific 3a	1.95					
32	NM_199534	<i>zgc:65851</i>	<i>zgc:65851</i>	1.94					
33	NM_001008648	<i>foxj1b</i>	forkhead box J1b	1.93	otic vesicle, lateral mesoderm ⁴⁶				
34	NM_001014333	<i>cdcp1a</i>	CUB domain containing protein 1a	1.90					
35	NM_131166	<i>hoxd10a</i>	homeobox D10a	1.90	tailbud	AP patterning ⁴⁰	AP patterning, myogenesis		Yes
36	NM_131690	<i>atp1a1b</i>	ATPase, Na+/K+ transporting, alpha 1b polypeptide (atp1a1b)	1.89					
37	NM_213118	<i>sox2</i>	SRY (sex determining region Y)-box 2	1.79	neural plate, tailbud ¹		epithelial-mesenchymal transition		
38	NM_001001402	<i>enc3</i>	ectodermal-neural cortex 3	1.79	lateral mesoderm, tailbud ²⁷	AP patterning ⁴⁷			
39	NM_001193651	<i>ctnnnd2b</i>	catenin (cadherin-associated protein), delta 2b	1.75					
40	NM_001006021	<i>amt</i>	aminomethyltransferase	1.73	yolk syncytial layer ¹³				
41	NM_214816	<i>tcf12</i>	transcription factor 12	1.72	adaxial, lateral mesoderm		myogenesis		Yes
42	NM_131146	<i>cyp26a1</i>	cytochrome P450, family 26, subfamily A, polypeptide 1	1.72	tailbud, anterior region	AP patterning ⁴⁸	AP patterning, somitogenesis		Yes
43	NM_131126	<i>hoxd9a</i>	homeobox D9a	1.71	tailbud	AP patterning ⁴⁰	AP patterning, myogenesis		Yes
44	NM_001077370	<i>prkar2aa</i>	protein kinase, cAMP-dependent, regulatory, type II, alpha A	1.70			epithelial-mesenchymal transition		
45	NM_131070	<i>mdka</i>	midkine a	1.69	paraxial mesoderm ⁴⁹		epithelial-mesenchymal transition		
46	NM_001030074	<i>kcnk6</i>	potassium channel, subfamily K, member 6	1.67	yolk syncytial layer, notochord ¹³				
47	NM_130971	<i>lfng</i>	LFNG O-fucosylpeptide 3-beta-N-acetylglucosaminyltransferase	1.64	neural plate, neural tube ¹³		somitogenesis		
48	NM_131541	<i>hoxb10a</i>	homeobox B10a	1.64	tailbud	AP patterning ⁴⁰			Yes
49	NM_200111	<i>arhgap29b</i>	Rho GTPase activating protein 29b	1.62	periderm, tailbud ¹				
50	NM_001030098	<i>prickle1b</i>	prickle homolog 1b	1.60	tailbud, axial mesoderm ⁹	AP patterning ⁵⁰			
51	NM_131125	<i>hoxd3a</i>	homeobox D3a	1.60	tailbud	AP patterning ⁴⁰	AP patterning		Yes
52	NM_199643	<i>coro2a</i>	coronin, actin binding protein, 2A	1.58	neural plate, epidermis ¹³				
53	NM_131281	<i>fgf8a</i>	fibroblast growth factor 8a	1.58	margin, tailbud ¹	somitogenesis ⁵¹		Yes ⁵²	
54	NM_194388	<i>tuba1b</i>	tubulin, alpha 1b	1.54	trigeminal placode ¹				
55	NM_199733	<i>tsku</i>	tsukushi small leucine rich proteoglycan homolog (Xenopus laevis)	1.54	margin, tailbud ¹⁴				
56	NM_001190982	<i>tuba1a</i>	tubulin, alpha 1a	1.54	ubiquitous ¹³				
57	NM_001242996	<i>mthfd1l</i>	methylenetetrahydrofolate dehydrogenase (NADP+ dependent) 1-like	1.54					
58	NM_001077153	<i>zfp36l1a</i>	zinc finger protein 36, C3H type-like 1a	1.52	optic primordium,				

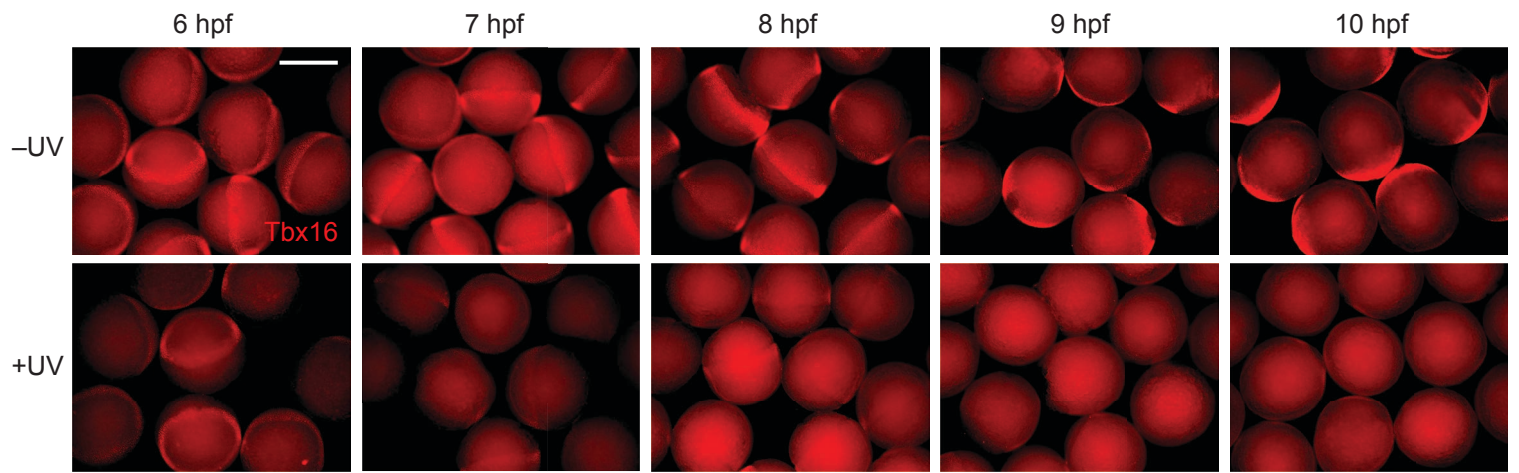
					tailbud ¹						
59	NM_213634	<i>ptgdsb</i>	prostaglandin D2 synthase b	1.52							
60	NM_199980	<i>itm2cb</i>	integral membrane protein 2Cb	1.50							

Supplementary Table 3. Phenotypic statistics (in order of presentation)

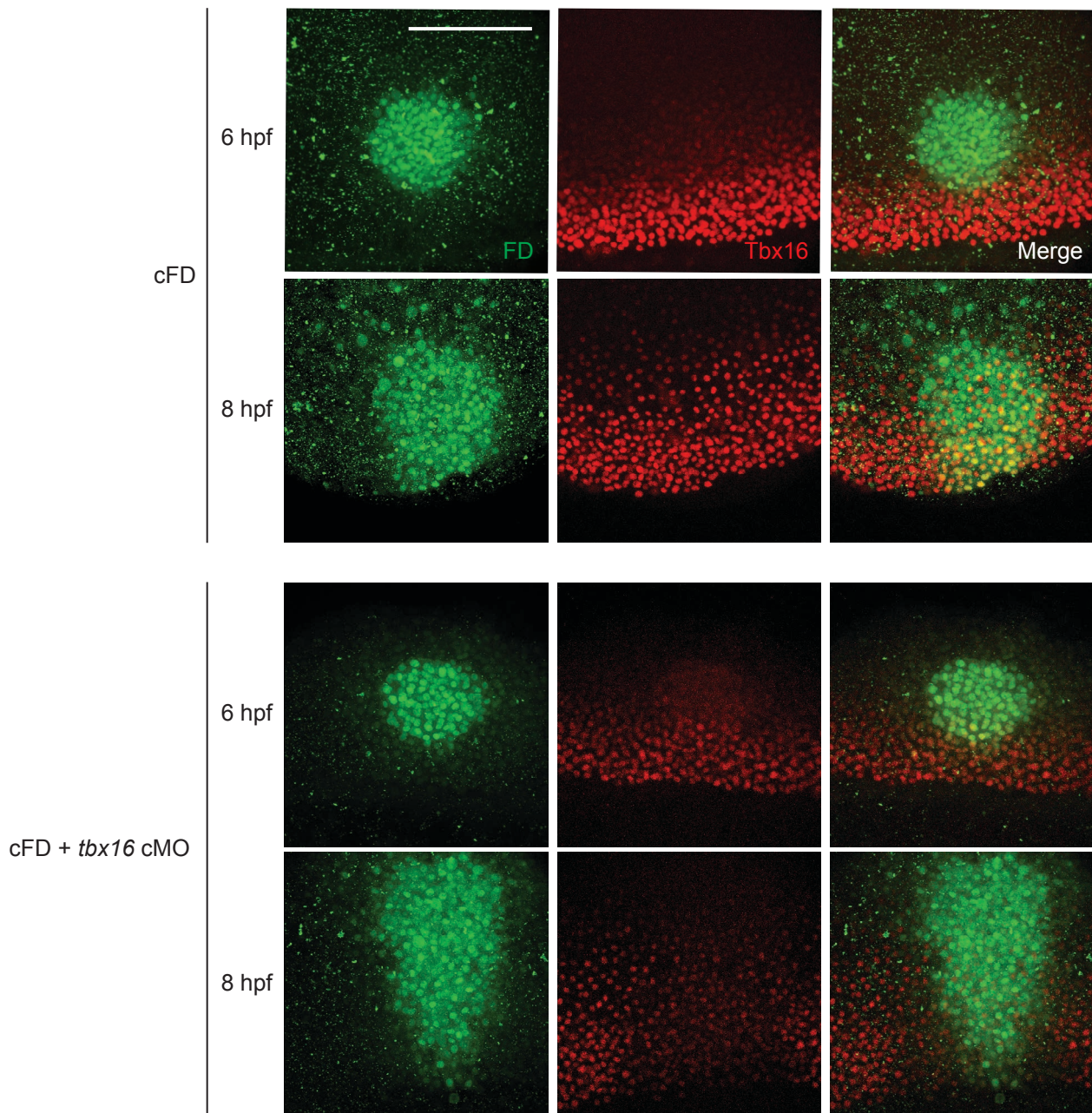
Figure	Micrograph	Phenotypic criteria	Total number of embryos	Number with phenotype	% Penetrance
Fig. 1b	<i>tbx16</i> cMO -UV	Trunk somites present; normal tailbud	12	12	100
Fig. 1b	<i>tbx16</i> cMO +UV	Loss of trunk somites; enlarged tailbud	13	13	100
Fig. 1e	cFD only	Ventral progenitors become trunk somites	19	19	100
Fig. 1e	cFD + <i>tbx16</i> cMO	Ventral progenitors located posteriorly	20	19	95
Fig. 3a	<i>hoxa9b</i> (8 hpf), WT	Expression in ventrolateral margin	11	0	0
Fig. 3a	<i>hoxa9b</i> (8 hpf), <i>tbx16</i> MO	Expression in ventrolateral margin	11	5	45
Fig. 3a	<i>hoxa9b</i> (10 hpf), WT	Weak expression in tailbud	7	7	100
Fig. 3a	<i>hoxa9b</i> (10 hpf), <i>tbx16</i> MO	Strong expression in tailbud	6	6	100
Fig. 3a	<i>hoxa9b</i> (13 hpf), WT	Strong expression in tailbud and paraxial mesoderm	7	7	100
Fig. 3a	<i>hoxa9b</i> (13 hpf), <i>tbx16</i> MO	Strong expression in tailbud and paraxial mesoderm	6	6	100
Fig. 3a	<i>hoxa10b</i> (8 hpf), WT	Expression in ventrolateral margin	13	0	0
Fig. 3a	<i>hoxa10b</i> (8 hpf), <i>tbx16</i> MO	Expression in ventrolateral margin	11	0	0
Fig. 3a	<i>hoxa10b</i> (10 hpf), WT	Expression in tailbud	7	0	0
Fig. 3a	<i>hoxa10b</i> (10 hpf), <i>tbx16</i> MO	Expression in tailbud	7	7	100
Fig. 3a	<i>hoxa10b</i> (13 hpf), WT	Expression in tailbud and paraxial mesoderm	7	7	100
Fig. 3a	<i>hoxa10b</i> (13 hpf), <i>tbx16</i> MO	Strong expression in tailbud and paraxial mesoderm	7	7	100
Fig. 3a	<i>hoxa13b</i> (8 hpf), WT	Expression in ventrolateral margin	10	0	0
Fig. 3a	<i>hoxa13b</i> (8 hpf), <i>tbx16</i> MO	Expression in ventrolateral margin	11	10	91
Fig. 3a	<i>hoxa13b</i> (10 hpf), WT	Expression in tailbud	15	0	0
Fig. 3a	<i>hoxa13b</i> (10 hpf), <i>tbx16</i> MO	Expression in tailbud	12	11	92
Fig. 3a	<i>hoxa13b</i> (13 hpf), WT	Weak expression in tailbud	16	15	94
Fig. 3a	<i>hoxa13b</i> (13 hpf), <i>tbx16</i> MO	Strong expression in tailbud	13	13	100
Fig. 3a	<i>hoxb6a</i> (8 hpf), WT	Expression in ventrolateral margin	13	9	69
Fig. 3a	<i>hoxb6a</i> (8 hpf), <i>tbx16</i> MO	Expression in ventrolateral margin	10	9	90
Fig. 3a	<i>hoxb6a</i> (10 hpf), WT	Expression in tailbud	18	18	100
Fig. 3a	<i>hoxb6a</i> (10 hpf), <i>tbx16</i> MO	Expression in tailbud	13	13	100
Fig. 3a	<i>hoxb6a</i> (13 hpf), WT	Expression in tailbud and paraxial mesoderm	14	14	100
Fig. 3a	<i>hoxb6a</i> (13 hpf), <i>tbx16</i> MO	Expression in tailbud and paraxial mesoderm	12	12	100
Fig. 3a	<i>hoxb10a</i> (8 hpf), WT	Expression in ventrolateral margin	10	4	40
Fig. 3a	<i>hoxb10a</i> (8 hpf), <i>tbx16</i> MO	Expression in ventrolateral margin	8	6	75
Fig. 3a	<i>hoxb10a</i> (10 hpf), WT	Expression in tailbud	7	7	100
Fig. 3a	<i>hoxb10a</i> (10 hpf), <i>tbx16</i> MO	Elevated expression in tailbud	6	6	100
Fig. 3a	<i>hoxb10a</i> (13 hpf), WT	Expression in tailbud and paraxial mesoderm	8	8	100
Fig. 3a	<i>hoxb10a</i> (13 hpf), <i>tbx16</i> MO	Expression in tailbud and paraxial mesoderm	6	6	100
Fig. 3a	<i>hoxc10a</i> (8 hpf), WT	Expression in ventrolateral margin	10	1	10
Fig. 3a	<i>hoxc10a</i> (8 hpf), <i>tbx16</i> MO	Expression in ventrolateral margin	11	8	73
Fig. 3a	<i>hoxc10a</i> (10 hpf), WT	Expression in tailbud	14	0	0
Fig. 3a	<i>hoxc10a</i> (10 hpf), <i>tbx16</i> MO	Expression in tailbud	11	11	100
Fig. 3a	<i>hoxc10a</i> (13 hpf), WT	Expression in tailbud	15	15	100
Fig. 3a	<i>hoxc10a</i> (13 hpf), <i>tbx16</i> MO	Expression in tailbud and paraxial mesoderm	13	13	100
Fig. 3a	<i>hoxd9a</i> (8 hpf), WT	Expression in ventrolateral margin	8	0	0
Fig. 3a	<i>hoxd9a</i> (8 hpf), <i>tbx16</i> MO	Expression in ventrolateral margin	10	0	0
Fig. 3a	<i>hoxd9a</i> (10 hpf), WT	Expression in tailbud	13	0	0
Fig. 3a	<i>hoxd9a</i> (10 hpf), <i>tbx16</i> MO	Expression in tailbud	13	12	92
Fig. 3a	<i>hoxd9a</i> (13 hpf), WT	Expression in tailbud	15	15	100
Fig. 3a	<i>hoxd9a</i> (13 hpf), <i>tbx16</i> MO	Expression in tailbud	13	13	100
Fig. 3a	<i>hoxd10a</i> (8 hpf), WT	Expression in ventrolateral margin	11	0	0
Fig. 3a	<i>hoxd10a</i> (8 hpf), <i>tbx16</i> MO	Expression in ventrolateral margin	8	1	13

Fig. 3a	<i>hoxd10a</i> (10 hpf), WT	Expression in tailbud	14	0	0
Fig. 3a	<i>hoxd10a</i> (10 hpf), <i>tbx16</i> MO	Expression in tailbud	13	11	85
Fig. 3a	<i>hoxd10a</i> (13 hpf), WT	Expression in tailbud	14	14	100
Fig. 3a	<i>hoxd10a</i> (13 hpf), <i>tbx16</i> MO	Expression in tailbud	15	15	100
Fig. 4a	cFD only	Upregulation of <i>hoxa9b</i> in irradiated cells	16	1	6
Fig. 4a	cFD + <i>tbx16</i> cMO	Upregulation of <i>hoxa9b</i> in irradiated cells and flanking tissues	12	10	83
Fig. 4b	<i>bmp2a</i> , WT	No detectable expression	34	30	88
Fig. 4b	<i>bmp2a</i> , <i>tbx16</i> MO	Expression in ventrolateral margin	26	25	96
Fig. 4b	<i>fsta</i> , WT	Strong expression in anterior mesoderm	35	32	91
Fig. 4b	<i>fsta</i> , <i>tbx16</i> MO	Reduced expression in anterior mesoderm	28	28	100
Fig. 4c	0 µM dorsomorphin	Precocious expression of <i>hoxa13b</i>	14	14	100
Fig. 4c	10 µM dorsomorphin	Precocious expression of <i>hoxa13b</i> , slightly weaker	12	12	100
Fig. 4c	25 µM dorsomorphin	Precocious expression of <i>hoxa13b</i> , faint	13	3	23
Fig. 4c	50 µM dorsomorphin	Precocious expression of <i>hoxa13b</i>	14	0	0
Fig. 5b	<i>mCherry-NLS</i>	EGFP observed in trunk somites	36	26	72
Fig. 5b	<i>hoxa13b</i>	EGFP observed in trunk somites	26	0	0
Fig. 5b	<i>hoxa13b</i> mutant	EGFP observed in trunk somites	33	23	70
Supp. Fig. 7a	<i>msgn1</i> , WT	Strong expression in tailbud	5	5	100
Supp. Fig. 7a	<i>msgn1</i> , <i>tbx16</i> MO	Reduced expression in tailbud	5	5	100
Supp. Fig. 7a	<i>tbx6l</i> , WT	Strong expression in tailbud	18	18	100
Supp. Fig. 7a	<i>tbx6l</i> , <i>tbx16</i> MO	Reduced expression in tailbud	13	13	100
Supp. Fig. 7a	<i>fzd10</i> , WT	Strong expression in tailbud	20	20	100
Supp. Fig. 7a	<i>fzd10</i> , <i>tbx16</i> MO	Reduced expression in tailbud	15	13	87
Supp. Fig. 7a	<i>rem1</i> , WT	Strong expression in tailbud and paraxial mesoderm	18	18	100
Supp. Fig. 7a	<i>rem1</i> , <i>tbx16</i> MO	Reduced expression in tailbud and paraxial mesoderm	15	15	100
Supp. Fig. 7a	<i>atp2a2a</i> , WT	Strong expression in tailbud and head	18	18	100
Supp. Fig. 7a	<i>atp2a2a</i> , <i>tbx16</i> MO	Reduced expression in tailbud and head	15	15	100
Supp. Fig. 7b	<i>adam8a</i> , WT	Expression in tailbud	18	18	100
Supp. Fig. 7b	<i>adam8a</i> , <i>tbx16</i> MO	Elevated expression in tailbud	15	13	87
Supp. Fig. 7b	<i>bmp2a</i> , WT	Weak expression in tailbud	15	15	100
Supp. Fig. 7b	<i>bmp2a</i> , <i>tbx16</i> MO	Strong expression in tailbud	12	12	100
Supp. Fig. 7b	<i>hivep2a</i> , WT	Weak expression in tailbud	18	18	100
Supp. Fig. 7b	<i>hivep2a</i> , <i>tbx16</i> MO	Strong expression in tailbud	15	13	87
Supp. Fig. 7b	<i>s1pr1</i> , WT	No detectable expression in tailbud	19	19	100
Supp. Fig. 7b	<i>s1pr1</i> , <i>tbx16</i> MO	Expression in tailbud	15	15	100
Supp. Fig. 7b	<i>tagln3b</i> , WT	Expression in tailbud	20	20	100
Supp. Fig. 7b	<i>tagln3b</i> , <i>tbx16</i> MO	Elevated expression in tailbud	15	14	93
Supp. Fig. 7b	<i>hoxd3a</i> , WT	Expression in tailbud	14	14	100
Supp. Fig. 7b	<i>hoxd3a</i> , <i>tbx16</i> MO	Elevated expression in tailbud	12	12	100
Supp. Fig. 7b	<i>cyp26a1</i> , WT	Expression in tailbud and anterior mesoderm	19	19	100
Supp. Fig. 7b	<i>cyp26a1</i> , <i>tbx16</i> MO	Elevated expression in tailbud and anterior mesoderm	16	14	88
Supp. Fig. 7b	<i>tcf12</i> , WT	Expression in anterior, paraxial mesoderm	18	18	100
Supp. Fig. 7b	<i>tcf12</i> , <i>tbx16</i> MO	Increased expression in tailbud and anterior mesoderm; loss of expression in adaxial and lateral mesoderm	13	11	85
Supp. Fig. 8	<i>actc1a</i> , WT	Adaxial expression	21	21	100
Supp. Fig. 8	<i>actc1a</i> , <i>tbx16</i> MO	Loss of adaxial expression	14	12	86
Supp. Fig. 8	<i>cxcl12a</i> , WT	Paraxial expression	5	5	100
Supp. Fig. 8	<i>cxcl12a</i> , <i>tbx16</i> MO	Loss of paraxial expression	5	5	100
Supp. Fig. 8	<i>foxc1b</i> , WT	Adaxial and tailbud expression	5	5	100
Supp. Fig. 8	<i>foxc1b</i> , <i>tbx16</i> MO	Reduced adaxial and tailbud expression	5	5	100
Supp. Fig. 8	<i>fsta</i> , WT	Anterior paraxial mesoderm expression	20	20	100
Supp. Fig. 8	<i>fsta</i> , <i>tbx16</i> MO	Reduced anterior paraxial mesoderm expression	15	15	100
Supp. Fig. 8	<i>mespab</i> , WT	Expression in forming somite	19	19	100
Supp. Fig. 8	<i>mespab</i> , <i>tbx16</i> MO	Loss of expression in forming somite; some adaxial expression	12	12	100

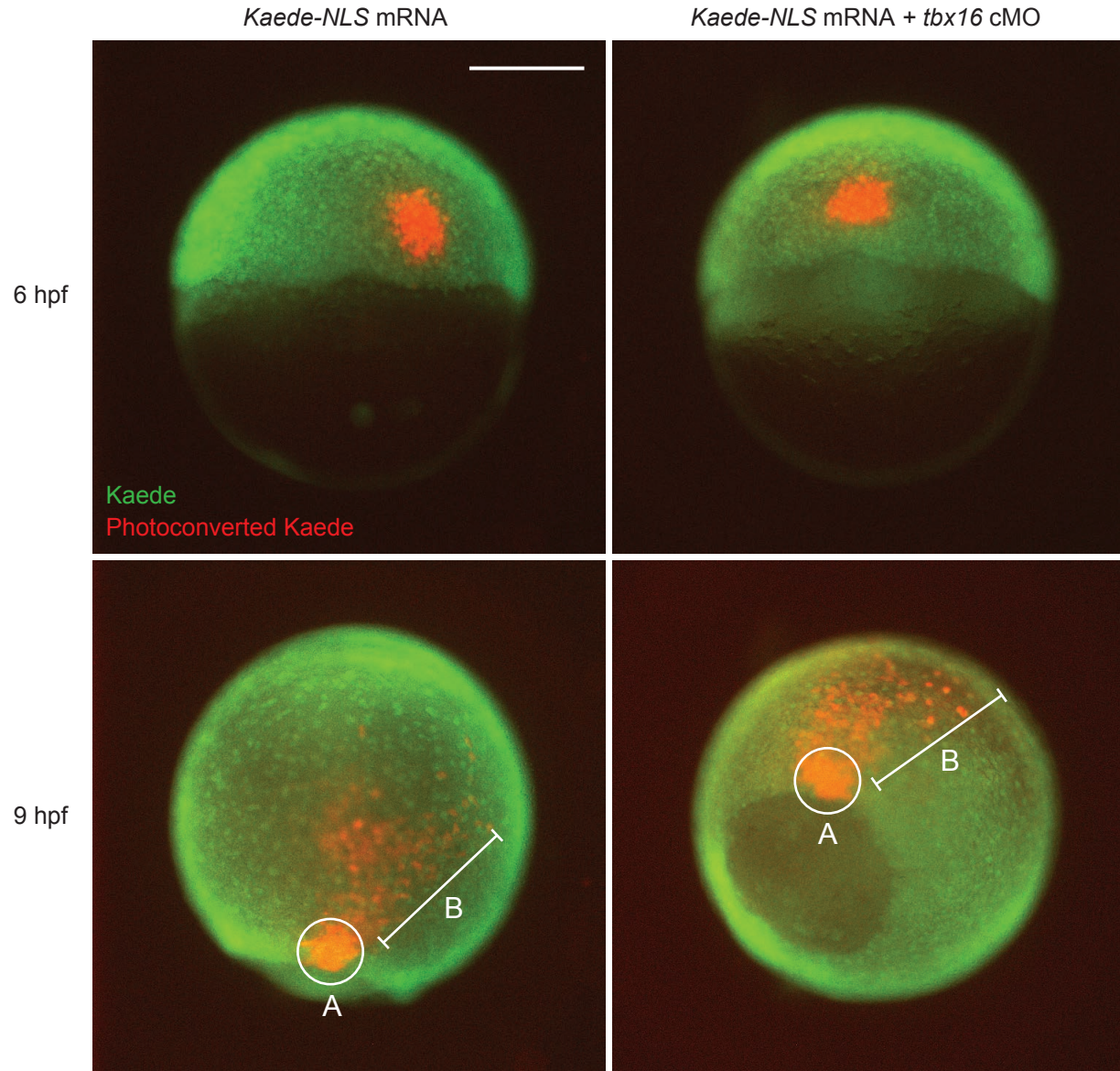
Supp. Fig. 8	<i>notch2</i> , WT	Axial and paraxial mesoderm expression	20	20	100
Supp. Fig. 8	<i>notch2</i> , <i>tbx16</i> MO	Reduced axial and loss of paraxial mesoderm expression	15	15	100
Supp. Fig. 8	<i>pcdh10b</i> , WT	Paraxial mesoderm expression	5	5	100
Supp. Fig. 8	<i>pcdh10b</i> , <i>tbx16</i> MO	Loss of paraxial mesoderm expression; ectopic expression in axial domain	5	5	100
Supp. Fig. 8	<i>ripply2</i> , WT	Expression in forming somite	19	19	100
Supp. Fig. 8	<i>ripply2</i> , <i>tbx16</i> MO	No detectable expression	14	14	100
Supp. Fig. 8	<i>aplnra</i> , WT	Expression in adaxial mesoderm and anterior region	19	19	100
Supp. Fig. 8	<i>aplnra</i> , <i>tbx16</i> MO	Loss of expression in adaxial mesoderm; expression maintained anteriorly	15	15	100
Supp. Fig. 8	<i>aplnrb</i> , WT	Adaxial, lateral, and tailbud mesoderm expression	20	20	100
Supp. Fig. 8	<i>aplnrb</i> , <i>tbx16</i> MO	Loss of expression in adaxial, lateral mesoderm; elevated expression in tailbud	14	14	100
Supp. Fig. 8	<i>fzd7b</i> , WT	Expression in paraxial mesoderm and anterior region	20	20	100
Supp. Fig. 8	<i>fzd7b</i> , <i>tbx16</i> MO	Loss of expression in paraxial mesoderm; expression maintained in anterior region; ectopic expression in axial domain	11	10	91
Supp. Fig. 8	<i>her11</i> , WT	Cyclic expression in paraxial mesoderm; expression in anterior structures.	18	18	100
Supp. Fig. 8	<i>her11</i> , <i>tbx16</i> MO	Loss of paraxial expression; expression maintained in anterior structures.	15	15	100
Supp. Fig. 8	<i>meis1</i> , WT	Expression in paraxial mesoderm and anterior structures	20	20	100
Supp. Fig. 8	<i>meis1</i> , <i>tbx16</i> MO	Loss of expression in paraxial mesoderm; expression maintained in anterior structures	15	15	100
Supp. Fig. 9	<i>hoxa9b</i>	No detectable expression	34	9	26
Supp. Fig. 9	<i>hoxa9b</i>	Weak expression in ventral margin	34	17	50
Supp. Fig. 9	<i>hoxa9b</i>	Strong expression in ventrolateral margin	34	8	24
Supp. Fig. 9	<i>hoxa13b</i>	No detectable expression	34	25	73
Supp. Fig. 9	<i>hoxa13b</i>	Expression in ventral margin	34	9	26
Supp. Fig. 9	<i>hoxb10a</i>	Weak expression in germ ring	33	7	21
Supp. Fig. 9	<i>hoxb10a</i>	Strong expression in germ ring	33	27	79
Supp. Fig. 9	<i>hoxc10a</i>	No detectable expression	33	8	24
Supp. Fig. 9	<i>hoxc10a</i>	Expression in ventrolateral margin	33	25	76
Supp. Fig. 10	<i>hoxa10b</i> , WT	Expression in mesodermal and neural tissues	7	7	100
Supp. Fig. 10	<i>hoxa10b</i> , <i>tbx16</i> MO	Expression pattern disrupted in mesodermal tissues but maintained in neural tissues	6	6	100
Supp. Fig. 10	<i>hoxb10a</i> , WT	Expression in mesodermal and neural tissues	7	7	100
Supp. Fig. 10	<i>hoxb10a</i> , <i>tbx16</i> MO	Expression pattern disrupted in mesodermal tissues but maintained in neural tissues	6	6	100
Supp. Fig. 10	<i>hoxc10a</i> , WT	Expression in mesodermal and neural tissues	13	13	100
Supp. Fig. 10	<i>hoxc10a</i> , <i>tbx16</i> MO	Expression pattern disrupted in mesodermal tissues but maintained in neural tissues	12	12	100
Supp. Fig. 10	<i>hoxd10a</i> , WT	Expression in mesodermal and neural tissues	15	15	100
Supp. Fig. 10	<i>hoxd10a</i> , <i>tbx16</i> MO	Expression pattern disrupted in mesodermal tissues but maintained in neural tissues	10	10	100
Supp. Fig. 11	<i>bmp2a</i>	No detectable expression	34	8	24
Supp. Fig. 11	<i>bmp2a</i>	Expression in the entire germ ring, including the dorsal margin	34	18	53
Supp. Fig. 11	<i>bmp2a</i>	Expression in ventrolateral margin	34	8	24
Supp. Fig. 11	<i>fsta</i>	Strong expression in anterior mesoderm	32	24	75
Supp. Fig. 11	<i>fsta</i>	Reduced expression in anterior mesoderm	32	8	25
Supp. Fig. 11	<i>bmp2a</i> + <i>fsta</i>	No <i>bmp2a</i> expression and strong <i>fsta</i> expression	34	8	24
Supp. Fig. 11	<i>bmp2a</i> + <i>fsta</i>	<i>bmp2</i> expression in entire germ ring and strong <i>fsta</i> expression	34	19	56
Supp. Fig. 11	<i>bmp2a</i> + <i>fsta</i>	<i>bmp2</i> expression in ventrolateral margin and reduced <i>fsta</i> expression	34	7	21
Supp. Fig. 14b	<i>EGFP</i> only	EGFP-positive cells with Tbx16 expression	3	3	100
Supp. Fig. 14b	<i>hoxa13b</i>	EGFP-positive cells with Tbx16 expression; aggregation of EGFP-positive cells	3	3	100
Supp. Fig. 14b	<i>hoxa13b</i> mutant	EGFP-positive cells with Tbx16 expression	3	3	100



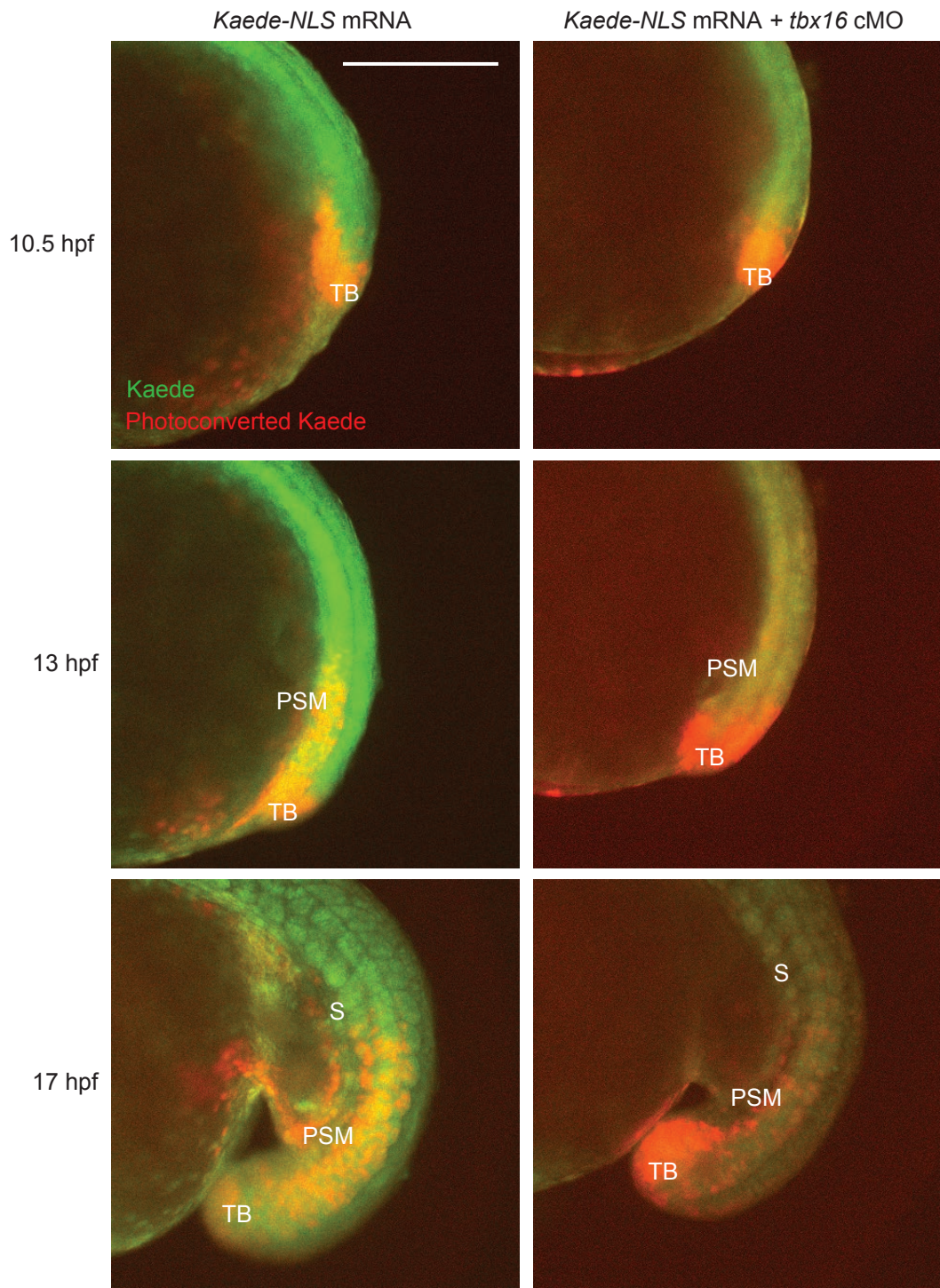
Supplementary Figure 1. Tbx16 protein turnover after global *tbx16* cMO photoactivation. Whole-mount immunostaining of Tbx16 protein in embryos injected with the *tbx16* cMO at the 1- to 4-cell stage and either cultured in the dark (-UV) or globally irradiated at 6 hpf (+UV). Tbx16 levels at the designated time points are shown, demonstrating maximum protein knockdown within 2-3 hours after cMO photoactivation. Scale bar: 500 μ m.



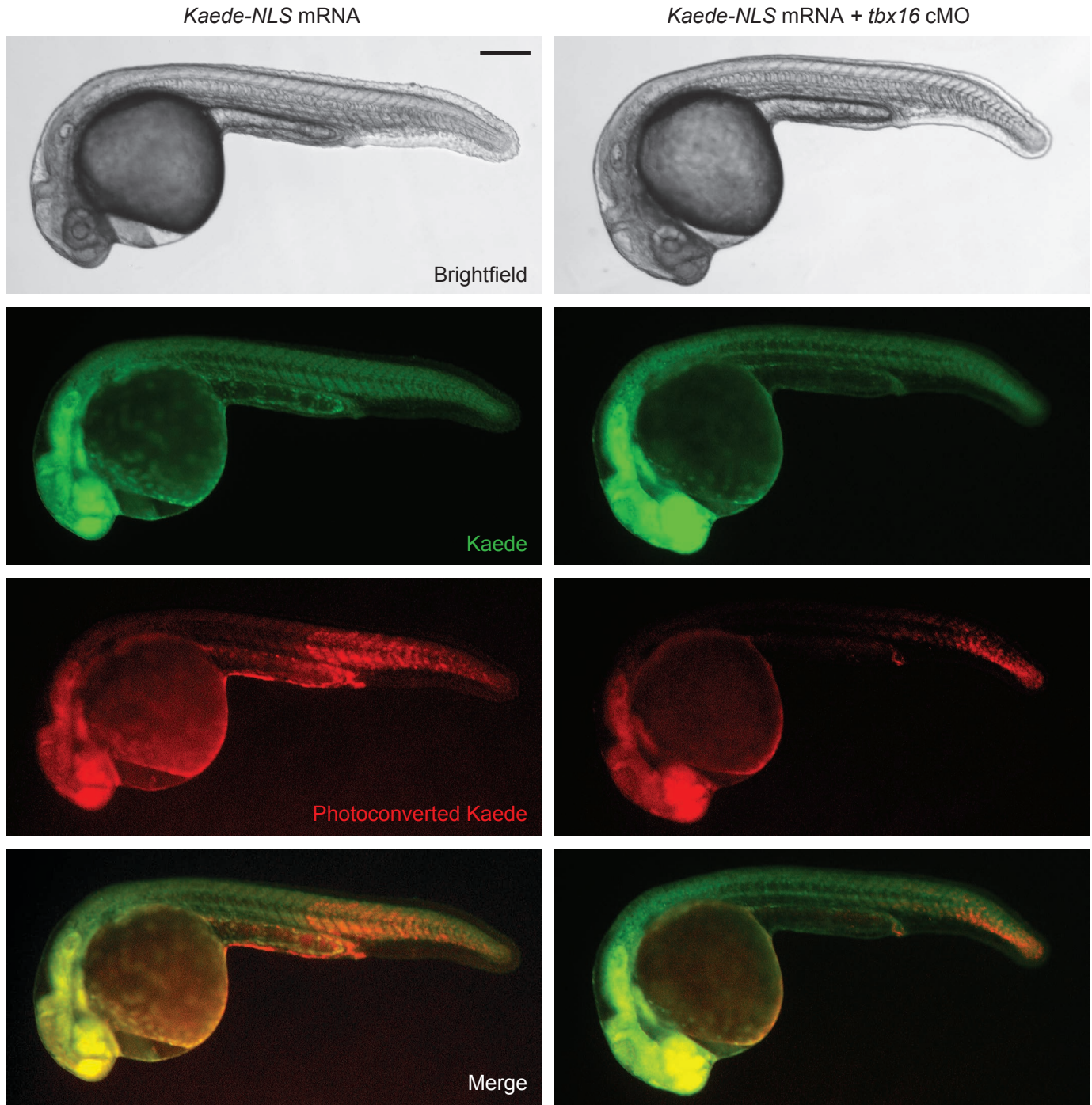
Supplementary Figure 2. Optochemical suppression of Tbx16 expression in ventral margin-derived MPCs. Co-immuno-staining of FD (green) and Tbx16 protein (red) in embryos injected with cFD or a cFD/tbx16 cMO mixture and then region-specifically irradiated within the ventral margin at 6 hpf. Tbx16 protein levels are significantly reduced in the optically targeted MPCs of cFD/tbx16 cMO-injected embryos at 8 hpf, whereas Tbx16 expression is unaffected in equivalently irradiated cFD-injected embryos. Embryo orientations: ventral view, animal pole up. Scale bar: 100 μ m.



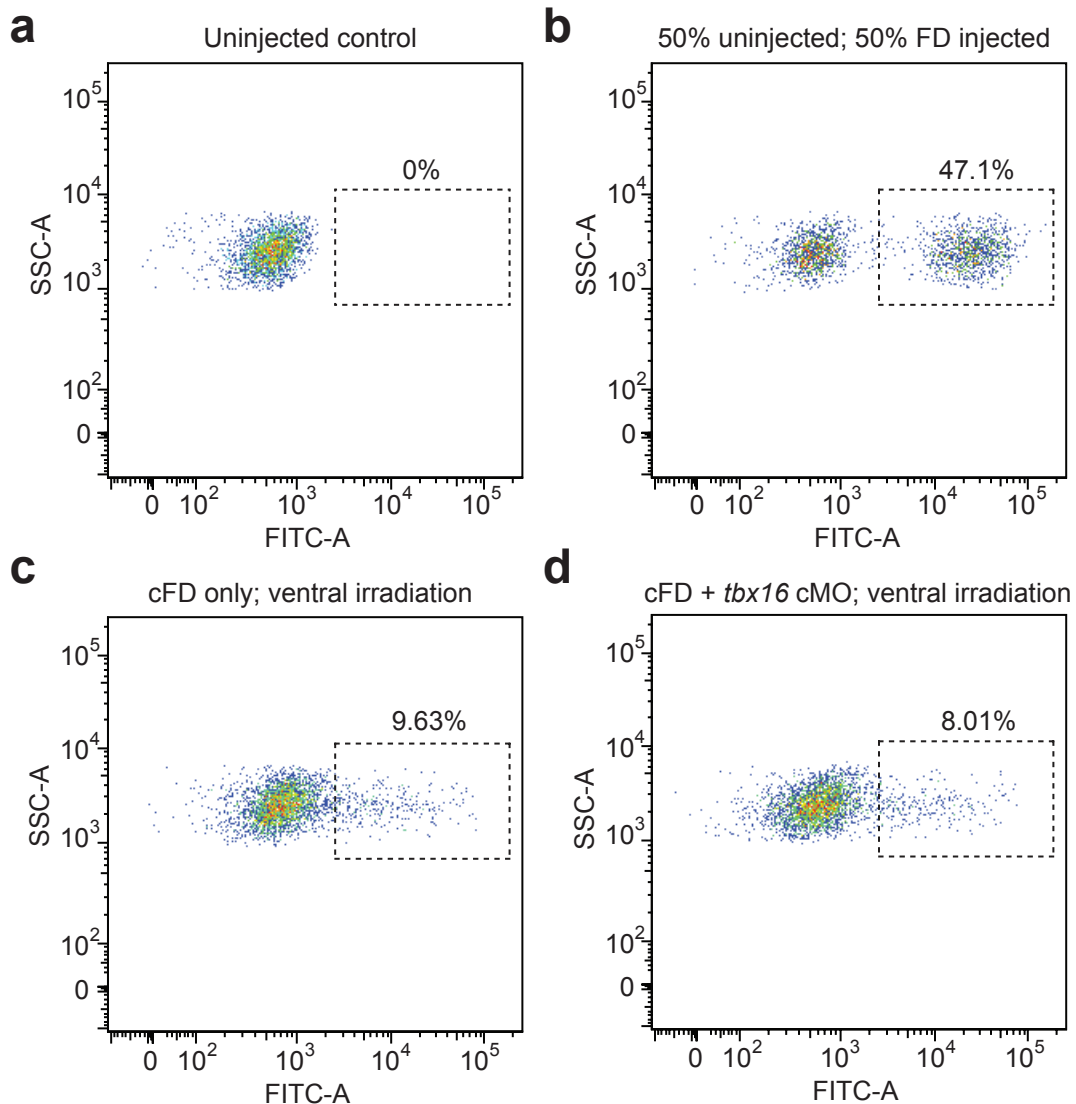
Supplementary Figure 3. Tbx16 knockdown does not alter the movement of ventral margin-derived cells during gastrulation. Zebrafish zygotes were injected with *Kaede-NLS* mRNA alone or in combination with the *tbx16* cMO and then spot-irradiated in the ventral margin at 6 hpf. Micrographs of representative embryos at 6 and 9 hpf are shown, revealing two cell populations with distinct migratory behaviors: A, epiblast cells that move directly to the margin; B, hypoblast cells that migrate toward the animal pole. Neither population exhibited Tbx16-dependent movements during this developmental phase. Embryo orientations: ventral view, animal pole up. Scale bar: 200 μ m. The depicted embryos are identical to those shown in Supplementary Figures 4 and 5, and complete time-lapse videos of these cell movements during gastrulation (6 to 9 hpf) are available as Supplementary Movie 1.



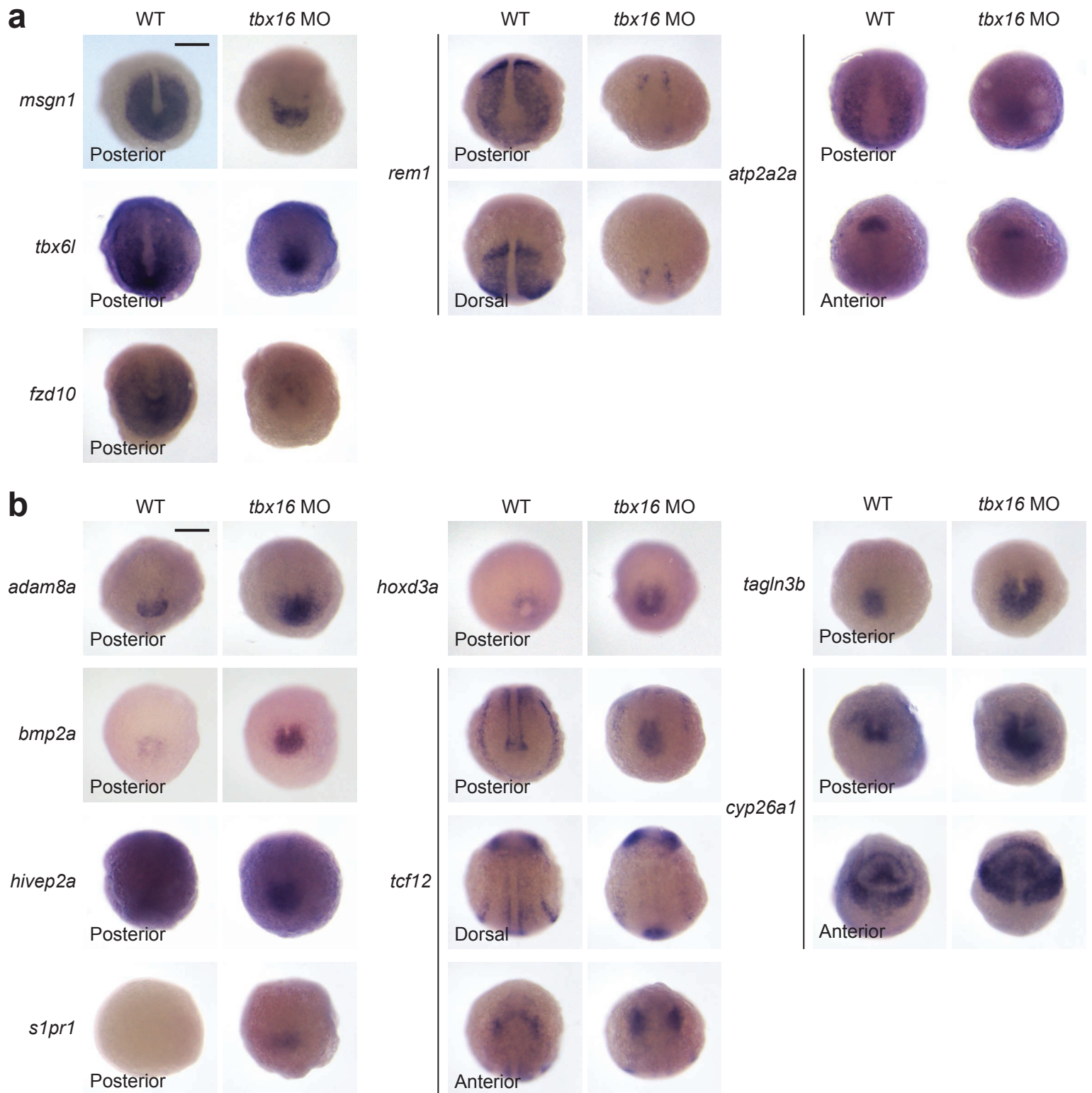
Supplementary Figure 4. Tbx16 knockdown inhibits egression of ventral margin-derived cells from the tailbud during early somitogenesis. Zebrafish zygotes were injected with *Kaede-NLS* mRNA alone or in combination with the *tbx16* cMO and then spot-irradiated in the ventral margin at 6 hpf. Micrographs of representative embryos at 10.5, 13, and 17 hpf are shown, demonstrating the *Tbx16*-dependent migration of ventral margin-derived MPCs from the tailbud into the presomitic mesoderm. Tailbud (TB), presomitic mesoderm (PSM), and somitic (S) tissues are labeled. Embryo orientations: lateral view, dorsal up, posterior right. Scale bar: 200 μ m. The depicted embryos are identical to those shown in Supplementary Figures 3 and 5, and complete time-lapse videos of these cell movements during early somitogenesis (10.5 to 17 hpf) are available as Supplementary Movie 2.



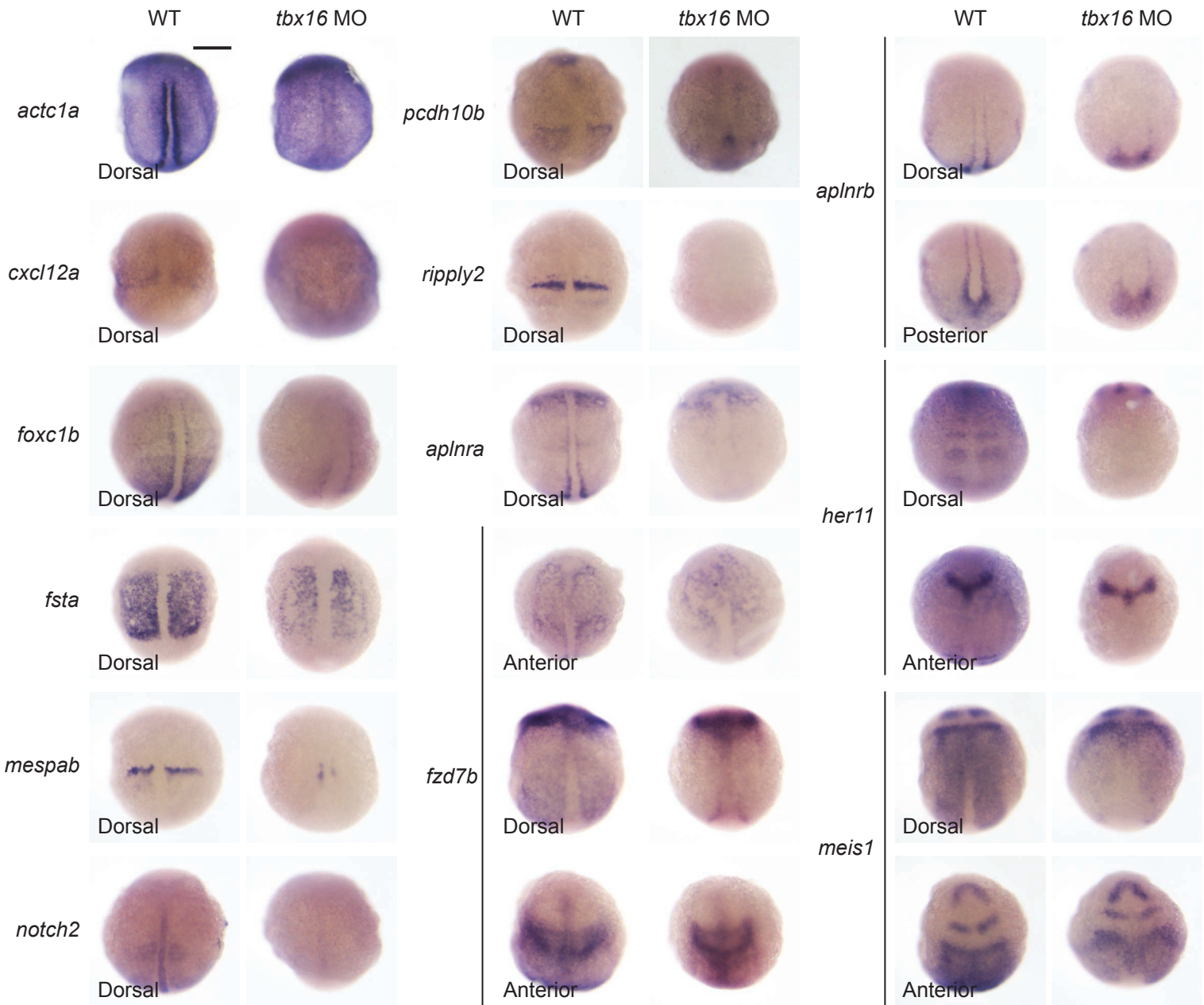
Supplementary Figure 5. Somite phenotypes associated with localized *Tbx16* knockdown in ventral margin-derived cells. Zebrafish zygotes were injected with *Kaede-NLS* mRNA alone or in combination with the *tbx16* cMO and then spot-irradiated in the ventral margin at 6 hpf. Micrographs of representative embryos at 24 hpf are shown, demonstrating the *Tbx16*-dependent differentiation of ventral margin-derived MPCs into trunk somitic muscle. Note that localized *Tbx16* knockdown does not cause significant changes in gross morphology. Embryo orientations: lateral view, anterior left. Scale bar: 200 μ m. The depicted embryos are identical to those shown in Supplementary Figures 3 and 4.



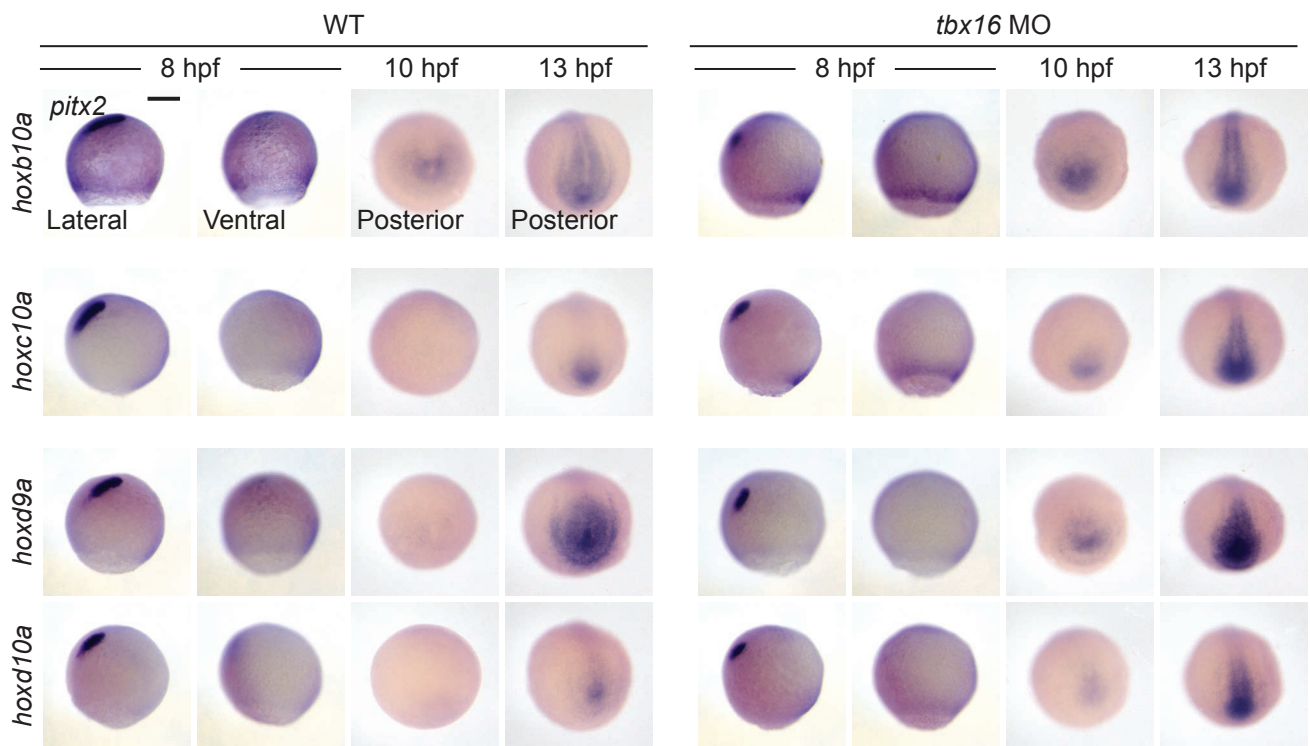
Supplementary Figure 6. Purification of irradiated ventral margin-derived cells by flow cytometry. Representative log-scale FACS plots obtained from embryos injected with cFD or a cFD/*tbx16* cMO mixture, spot-irradiated in the ventral margin, cultured until 9 hpf, and then dissociated into single cells. Fluorescence intensity (FITC-A: Ex: 488 nm, Em: 530 nm) and side-scatter area (SSC-A) measurements are shown for the following conditions: (a) uninjected embryos, (b) 1:1 ratio of uninjected embryos and FD-injected embryos; (c) spot-irradiated embryos injected with cFD alone, and (d) spot-irradiated embryos injected with a cFD/*tbx16* cMO mixture. The percentage of total cells within the sorting gate (dashed lines) for each condition is shown.



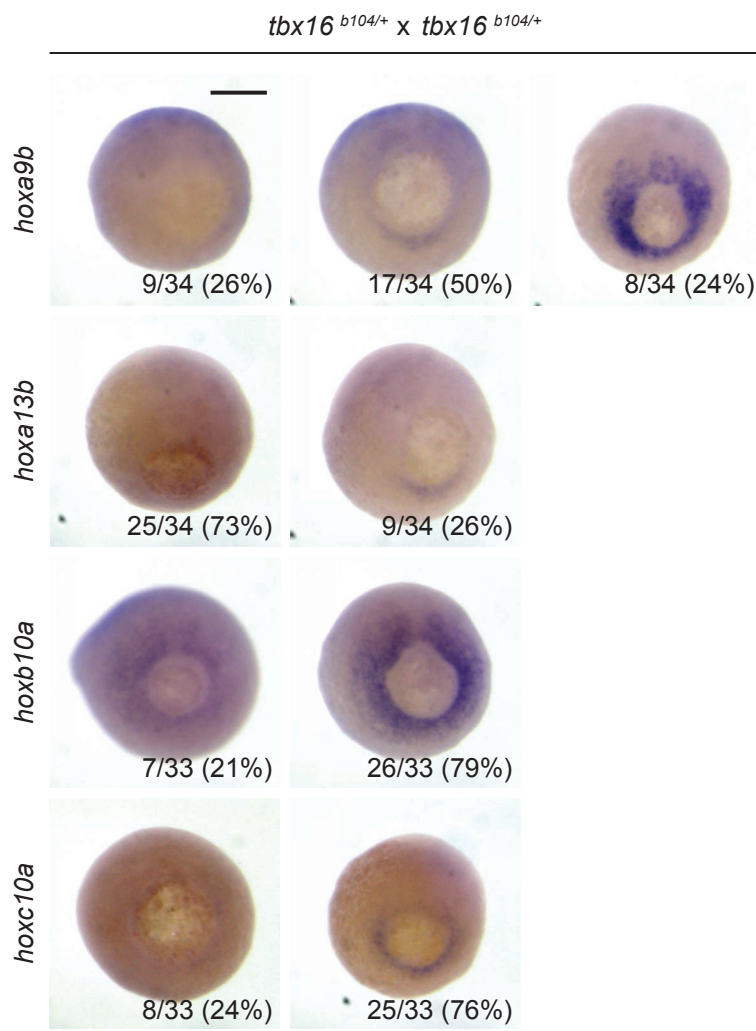
Supplementary Figure 7. Validation of selected Tbx16-dependent genes that are expressed in the tailbud. Analysis of candidate Tbx16 targets in wild type and *tbx16* morphant embryos by *in situ* hybridization. Genes that are downregulated (a) and upregulated (b) in *tbx16* morphants at 10-hpf are shown. Embryo orientations: posterior view, dorsal up; dorsal view, anterior up; or anterior view, dorsal down. Scale bar: 200 μ m.



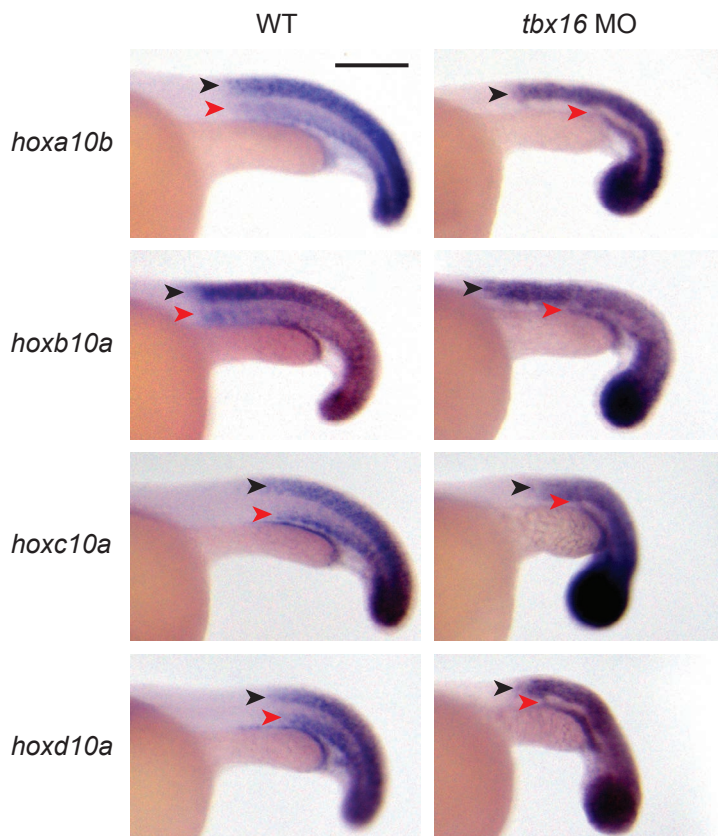
Supplementary Figure 8. Validation of selected Tbx16-dependent genes that are expressed in paraxial or adaxial mesoderm. Analysis of candidate Tbx16 targets in wild type and *tbx16* morphant embryos by *in situ* hybridization. Genes that are downregulated in *tbx16* morphants at 10 hpf are shown. Embryo orientations: posterior view, dorsal up; dorsal view, anterior up; or anterior view, dorsal down. Scale bar: 200 μ m.



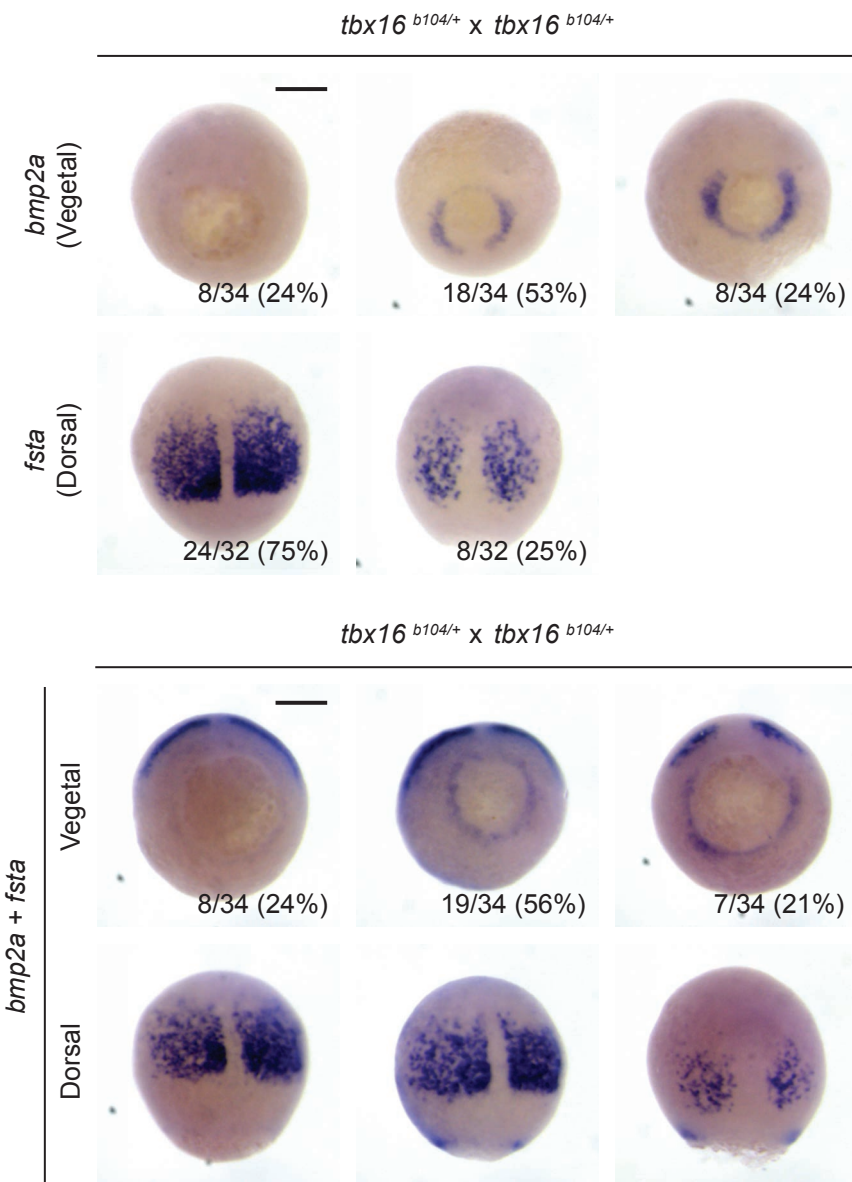
Supplementary Figure 9. Tbx16 regulates hox gene activation during gastrulation. (a) *hox* gene expression in wild type and *tbx16* morphant embryos during mid-gastrulation (8 hpf), tailbud formation (10 hpf), and early somitogenesis (13 hpf) as determined by *in situ* hybridization. Representative posterior *hox* genes identified in our transcriptome-wide survey for Tbx16 targets are shown. *pitx2* expression in the prechordal mesoderm was used as a dorsal marker. Embryo orientations: lateral view, dorsal left; ventral view, anterior up; and posterior view, dorsal up. Scale bar: 200 μ m.



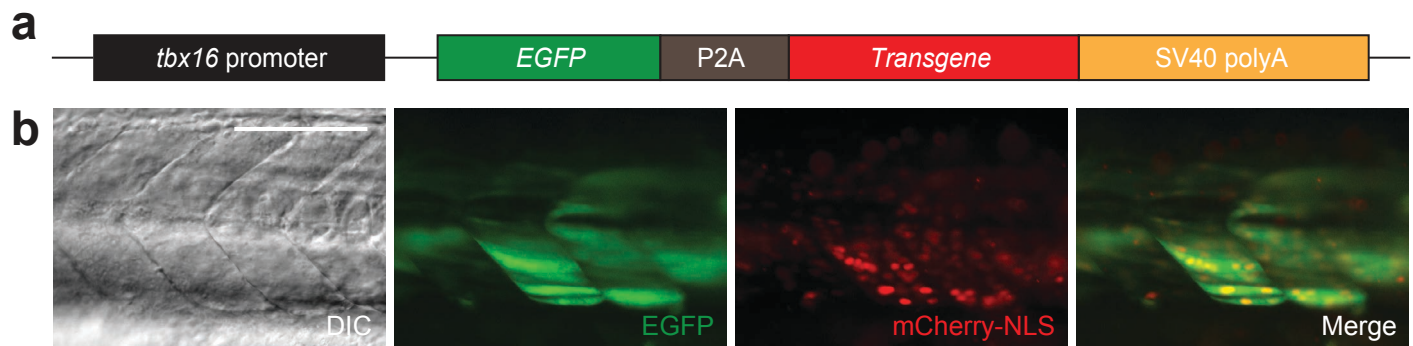
Supplementary Figure 10. Genetic loss of *tbx16* function upregulates posterior *hox* gene expression. Posterior *hox* gene expression patterns in progeny obtained by incrossing *tbx16* mutant heterozygotes. 9-hpf embryos are shown, and their phenotypic distributions reveal that wild type *tbx16* can be haploinsufficient with respect to its regulation of certain transcripts. Embryo orientations: posterior view, dorsal up. Scale bar: 200 μ m.



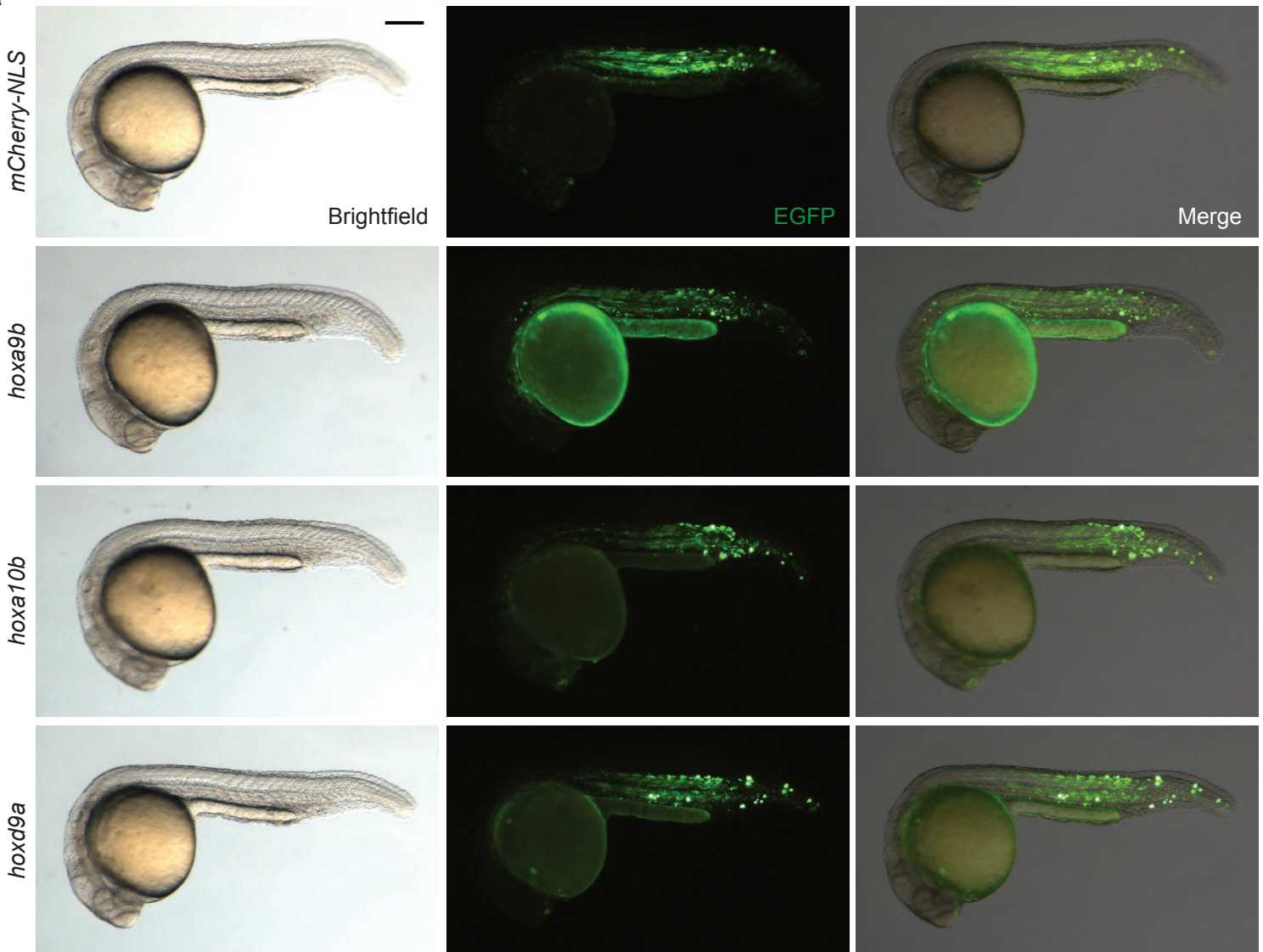
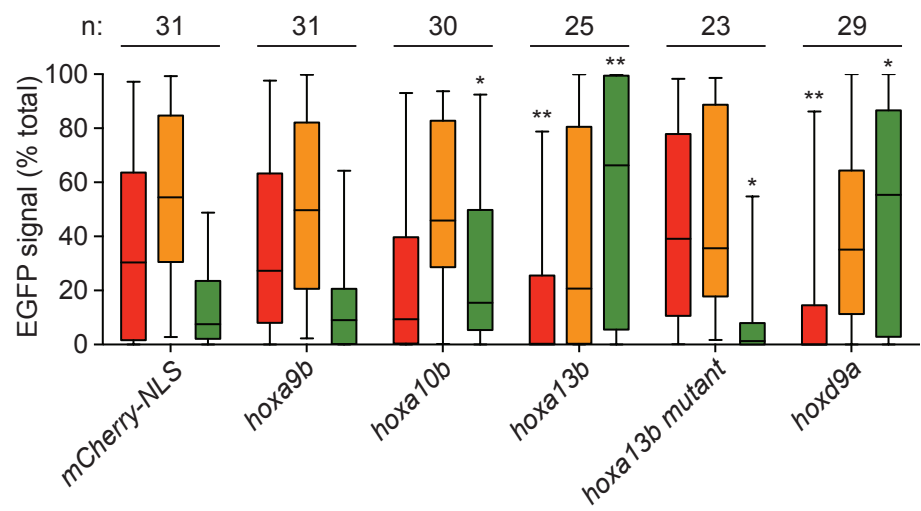
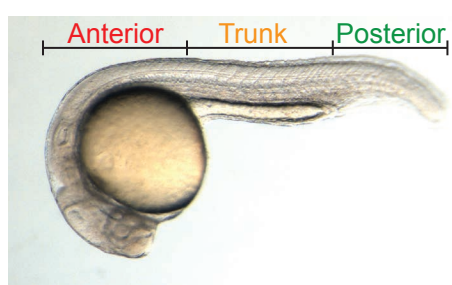
Supplementary Figure 11. Tbx16 regulates mesodermal but not neural *hox* gene activation. Comparison of posterior *hox* gene expression in wild type and *tbx16* morphant embryos by *in situ* hybridization. Expression patterns of selected group 10 paralogs in 24-hpf embryos are shown, and the anterior limits of neural and mesodermal transcription are labeled with black and red arrowheads, respectively. Embryo orientations: lateral view, anterior left. Scale bar: 200 μ m.



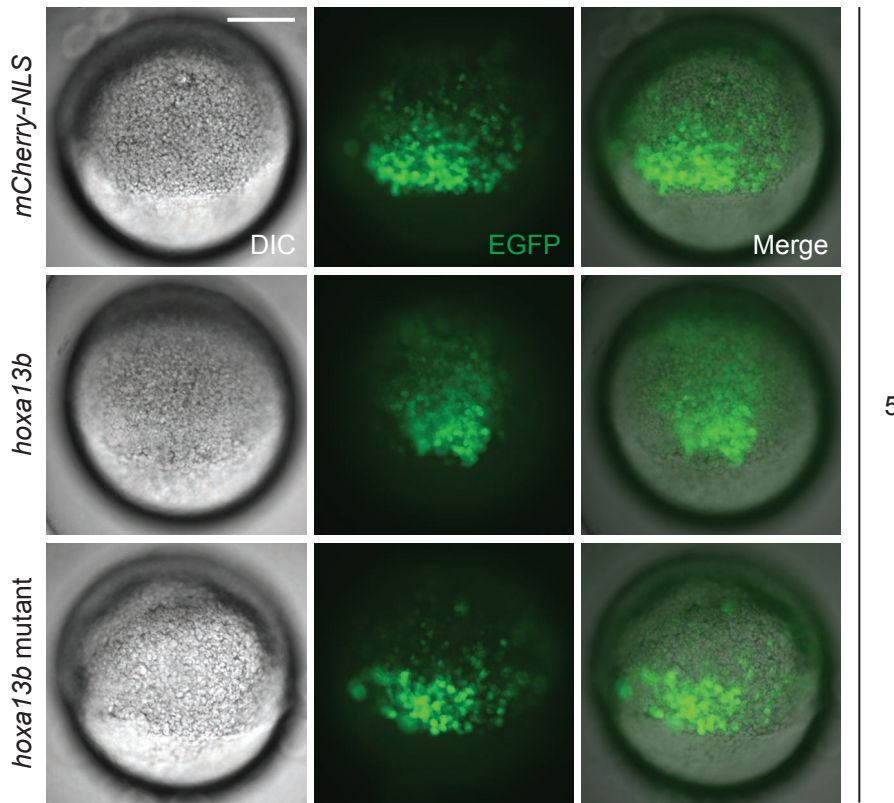
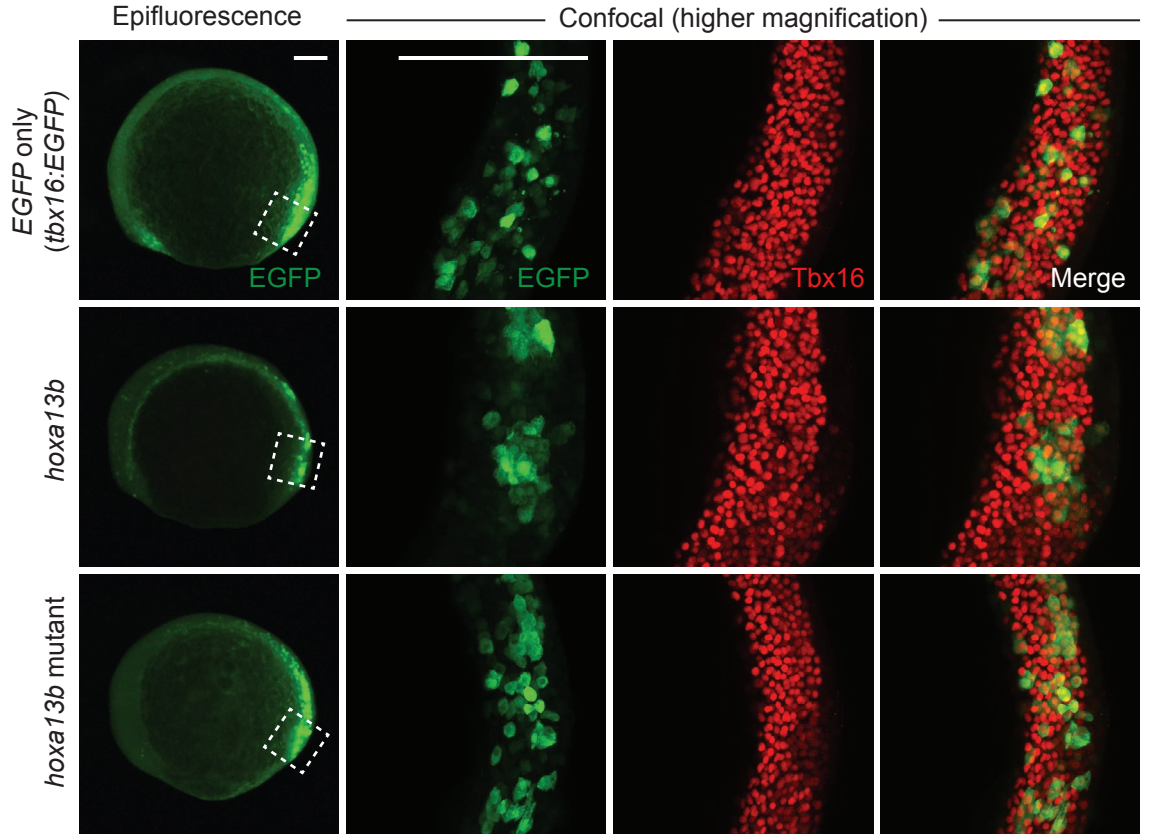
Supplementary Figure 12. Genetic loss of *tbx16* function upregulates BMP signaling. Expression of *bmp2a* and/or *fsta* in progeny obtained by incrossing *tbx16* mutant heterozygotes. 8-hpf embryos are shown, and their phenotypic distributions reveal that wild type *tbx16* is haploinsufficient with respect to *bmp2a* suppression. Embryo orientations: vegetal pole view, dorsal up; or dorsal view, animal pole up. Scale bars: 200 μm.



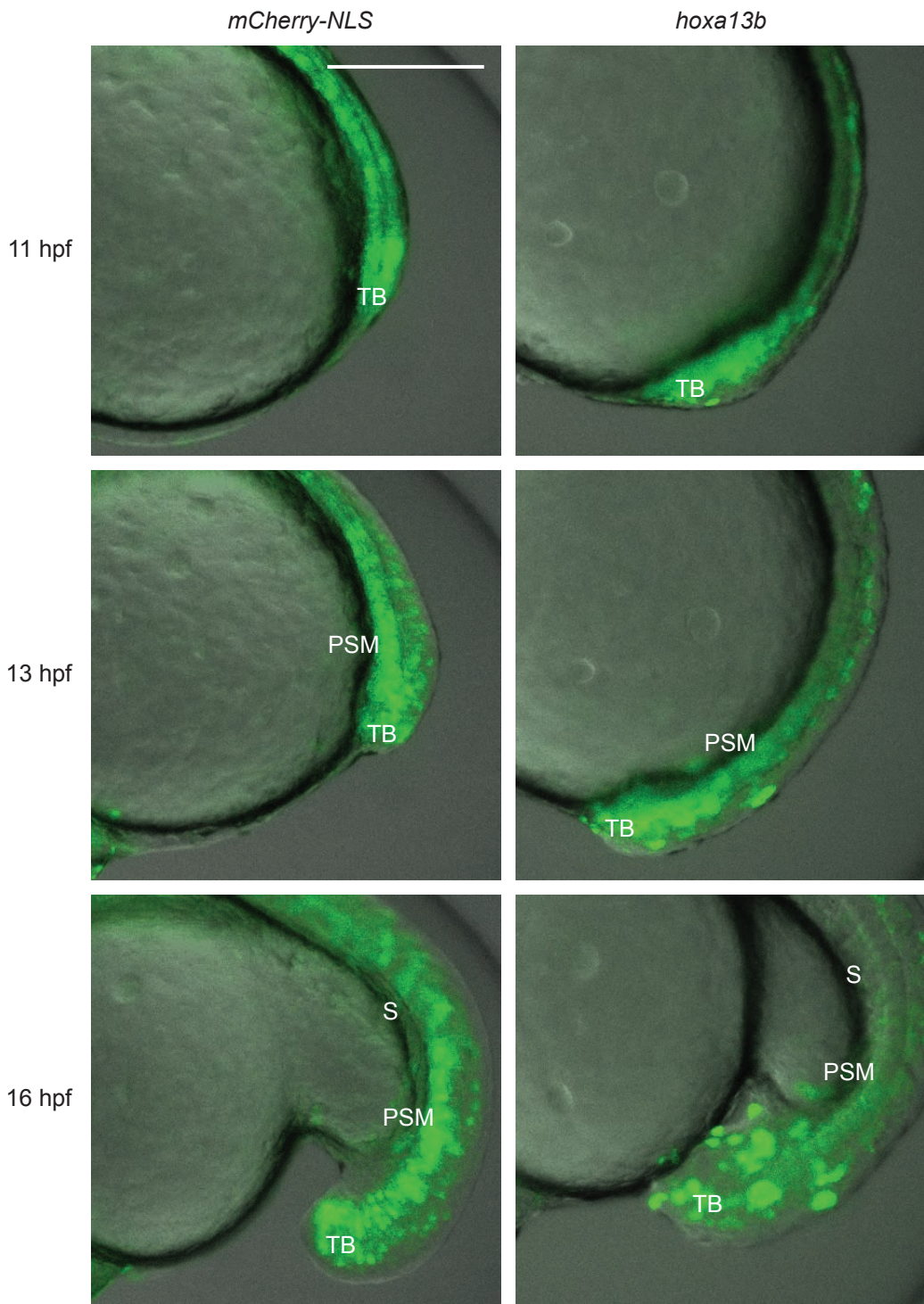
Supplementary Figure 13. Bicistronic expression of a *tbx16:EGFP-P2A-transgene* construct. (a) Construct used for MPC-targeted bicistronic expression of transgenes and an EGFP reporter. (b) Brightfield and fluorescence micrographs of zebrafish embryos injected with a pDestTol2-*tbx16:EGFP-P2A-mCherry-NLS* plasmid at the one-cell stage. The mosaic expression of cytoplasmic EGFP and nuclear mCherry-NLS in trunk somite cells at 24 hpf confirms mesoderm-specific expression and high-efficiency P2A linker “cleavage” via ribosomal skipping. Embryo orientations: lateral view, anterior left. Scale bar: 100 μ m.

a**b**

Supplementary Figure 14. Multiple posterior *hox* genes can alter paraxial MPC localization. (a) Representative anterior-posterior distributions of EGFP-positive cells in 22- to 24-hpf embryos injected with the designated *tbx16:EGFP-P2A-transgene* constructs at the 1- to 4-cell stage. (b) Anterior (red), trunk (orange), and posterior (green) regions of the body axis as delineated by the yolk extension boundaries and box-and-whisker plots of EGFP signals localized to each domain (excluding yolk cells) in the mosaic *tbx16:EGFP-P2A-transgene* embryos. Median values (horizontal lines), upper and lower quartiles (boxes), and maximum and minimum limits (whiskers) are shown. Five planned comparisons with the *mCherry-NLS* control were made for each region to obtain raw uncorrected *P*-values: *, *P* < 0.05; **, *P* < 0.01. Embryo orientations for a and b: lateral view, anterior left. Scale bar: 200 μ m.

a**b**

Supplementary Figure 15. *hoxa13b* overexpression inhibits MPC movement without disrupting Tbx16 expression. (a) Zebrafish zygotes were injected with *tbx16:EGFP-P2A-mCherry-NLS* or *tbx16:EGFP-P2A-hoxa13b* constructs and then tracked by differential interference contrast (DIC) and epifluorescence imaging throughout gastrulation. Robust Tbx16-dependent transgene expression could be observed by 5 hpf. (b) Epifluorescence and confocal imaging of immunostained mosaic embryos at 12 hpf, with regions demarcated by the dashed lines shown at higher magnification. Cells overexpressing *hoxa13b* retained the EGFP marker and maintained Tbx16 expression at this stage, by which point, they exhibit movement defects (see Supplementary Figure 16 and Supplementary Movie 3). Embryo orientations: a, margin view, animal pole up; b, lateral view, dorsal up. Scale bars: a, 200 μ m; b, 100 μ m.



Supplementary Figure 16. *hoxa13b* overexpression inhibits MPC egression from the tailbud during early somitogenesis. Zebrafish zygotes were injected with *tbx16:EGFP-P2A-mCherry-NLS* or *tbx16:EGFP-P2A-hoxa13b* constructs and then imaged during early somitogenesis. Micrographs of representative embryos at 11, 13, and 16 hpf are shown, demonstrating the *hoxa13b*-suppressed movement of MPCs from the tailbud into the presomitic mesoderm. Tailbud (TB), presomitic mesoderm (PSM), and somitic (S) tissues are labeled. Embryo orientations: lateral view, dorsal up, posterior right. Scale bar: 200 μ m. The complete time-lapse videos of these cell movements during early somitogenesis (10.5 to 16.25 hpf) are available as Supplementary Movie 3.

SUPPLEMENTARY MOVIES

Supplementary Movie 1. Ventral MPCs lacking Tbx16 function do not exhibit movement

defects during gastrulation. Time-lapse imaging of embryos injected with either *Kaede-NLS* mRNA alone or in combination with the *tbx16* cMO and spot-irradiated in the ventral margin at 6 hpf. Optically targeted cells can then be identified by the red fluorescence of photoconverted Kaede-NLS protein. Morphogenetic movements from 6 hpf to 9 hpf were imaged at a rate of 1 frame/5 minutes, and the movie is shown at a rate of 10 frames (50 minutes of development)/second. Embryo orientations: ventral view, animal pole up. Scale bar: 200 μ m. The same embryos were imaged at later stages to generate Supplementary Movie 2.

Supplementary Movie 2. Ventral MPCs lacking Tbx16 function exhibit movement defects

during somitogenesis. Time-lapse imaging of embryos injected with either *Kaede-NLS* mRNA alone or in combination with the *tbx16* cMO and spot-irradiated in the ventral margin at 6 hpf. Optically targeted cells can then be identified by the red fluorescence of photoconverted Kaede-NLS protein. Morphogenetic movements from 10.5 to 17 hpf were imaged at a rate of 1 frame/5 minutes, and movie is shown a rate of 10 frames (50 minutes of development)/second. Embryo orientations: lateral view, dorsal up. Scale bar: 200 μ m. The same embryos were imaged at earlier stages to generate Supplementary Movie 1.

Supplementary Movie 3. MPCs overexpressing *hoxa13b* exhibit movement defects during

somitogenesis. Time-lapse imaging of embryos injected with either *tbx16:EGFP-P2A-mCherry-NLS* or *tbx16:EGFP-P2A-hoxa13b-NLS* constructs at the 1- to 4-cell stage. Morphogenetic movements from 10.5 to 16.25 hpf were imaged at a rate of 1 frame/5 minutes, and movie is

shown a rate of 10 frames (50 minutes of development)/second. Embryo orientations: lateral view, dorsal up. Scale bar: 200 μ m.

REFERENCES

1. Thisse, B. *et al.* (2001) Expression of the zebrafish genome during embryogenesis (NIH R01 RR15402). ZFIN Direct Data Submission (<http://zfin.org>).
2. Murakami, T., Hijikata, T., Matsukawa, M., Ishikawa, H. & Yorifuji, H. Zebrafish protocadherin 10 is involved in paraxial mesoderm development and somitogenesis. *Dev. Dyn.* 235, 506-514 (2006).
3. Garnett, A.T. *et al.* Identification of direct T-box target genes in the developing zebrafish mesoderm. *Development* 136, 749-760 (2009).
4. Mueller, R.L., Huang, C. & Ho, R.K. Spatio-temporal regulation of Wnt and retinoic acid signaling by tbx16/spadetail during zebrafish mesoderm differentiation. *BMC Genomics* 11, 492 (2010).
5. Mishima, Y. *et al.* Zebrafish miR-1 and miR-133 shape muscle gene expression and regulate sarcomeric actin organization. *Genes Dev.* 23, 619-632 (2009).
6. Kawamura, A. *et al.* Groucho-associated transcriptional repressor ripply1 is required for proper transition from the presomitic mesoderm to somites. *Dev. Cell* 9, 735-744 (2005).
7. He, Y. *et al.* Maternal control of axial-paraxial mesoderm patterning via direct transcriptional repression in zebrafish. *Dev. Biol.* 386, 96-110 (2014).
8. Yamamoto, A. *et al.* Zebrafish paraxial protocadherin is a downstream target of spadetail involved in morphogenesis of gastrula mesoderm. *Development* 125, 3389-3397 (1998).
9. Thisse, B. & Thisse, C. (2005) High Throughput Expression Analysis of ZF-Models Consortium Clones. ZFIN Direct Data Submission (<http://zfin.org>).
10. Sieger, D., Tautz, D. & Gajewski, M. her11 is involved in the somitogenesis clock in zebrafish. *Dev. Genes Evol.* 214, 393-406 (2004).

11. Brown, J.L. *et al.* Transcriptional profiling of endogenous germ layer precursor cells identifies *dusp4* as an essential gene in zebrafish endoderm specification. *Proc. Natl. Acad. Sci. U. S. A.* 105, 12337-12342 (2008).
12. Hagos, E.G. & Dougan, S.T. Time-dependent patterning of the mesoderm and endoderm by Nodal signals in zebrafish. *BMC Dev. Biol.* 7, 22 (2007).
13. Thisse, B. & Thisse, C. (2004) Fast Release Clones: A High Throughput Expression Analysis. ZFIN Direct Data Submission (<http://zfin.org>).
14. Thisse, B., Wright, G.J. & Thisse, C. (2008) Embryonic and Larval Expression Patterns from a Large Scale Screening for Novel Low Affinity Extracellular Protein Interactions. ZFIN Direct Data Submission (<http://zfin.org>).
15. Fior, R. *et al.* The differentiation and movement of presomitic mesoderm progenitor cells are controlled by Mesogenin 1. *Development* 139, 4656-4665 (2012).
16. Yabe, T. & Takada, S. Mesogenin causes embryonic mesoderm progenitors to differentiate during development of zebrafish tail somites. *Dev. Biol.* 370, 213-222 (2012).
17. Bakkers, J. *et al.* *Has2* is required upstream of *Rac1* to govern dorsal migration of lateral cells during zebrafish gastrulation. *Development* 131, 525-537 (2004).
18. Ochi, H., Pearson, B.J., Chuang, P.T., Hammerschmidt, M. & Westerfield, M. *Hhip* regulates zebrafish muscle development by both sequestering Hedgehog and modulating localization of *Smoothened*. *Dev. Biol.* 297, 127-140 (2006).
19. Chong, S.W., Nguyet, L.M., Jiang, Y.J. & Korzh, V. The chemokine *Sdf-1* and its receptor *Cxcr4* are required for formation of muscle in zebrafish. *BMC Dev. Biol.* 7, 54 (2007).
20. Miyake, A. *et al.* Neucrin, a novel secreted antagonist of canonical Wnt signaling, plays roles in developing neural tissues in zebrafish. *Mech. Dev.* 128, 577-590 (2012).

21. Pezeron, G. *et al.* Duplicate sfrp1 genes in zebrafish: sfrp1a is dynamically expressed in the developing central nervous system, gut and lateral line. *Gene Expr. Patterns* 6, 835-842 (2006).
22. Topczewska, J.M. *et al.* The winged helix transcription factor Foxc1a is essential for somitogenesis in zebrafish. *Genes Dev.* 15, 2483-2493 (2001).
23. Yao, S. *et al.* Pnas4 is a novel regulator for convergence and extension during vertebrate gastrulation. *FEBS Lett.* 582, 2325-2332 (2008).
24. Costa, A.M. *et al.* GRG5/AES interacts with T-cell factor 4 (TCF4) and downregulates Wnt signaling in human cells and zebrafish embryos. *PLoS One* 8, e67694 (2013).
25. Feng, L., Hernandez, R.E., Waxman, J.S., Yelon, D. & Moens, C.B. Dhrs3a regulates retinoic acid biosynthesis through a feedback inhibition mechanism. *Dev. Biol.* 338, 1-14 (2010).
26. Begemann, G., Schilling, T.F., Rauch, G.J., Geisler, R. & Ingham, P.W. The zebrafish neckless mutation reveals a requirement for raldh2 in mesodermal signals that pattern the hindbrain. *Development* 128, 3081-3094 (2001).
27. Kudoh, T. *et al.* A gene expression screen in zebrafish embryogenesis. *Genome Res.* 11, 1979-1987 (2001).
28. Feldman, B. *et al.* Lefty antagonism of Squint is essential for normal gastrulation. *Curr. Biol.* 12, 2129-2135 (2002).
29. Draper, B.W., Stock, D.W. & Kimmel, C.B. Zebrafish fgf24 functions with fgf8 to promote posterior mesodermal development. *Development* 130, 4639-4654 (2003).
30. Wang, H. *et al.* Isolation and expression of zebrafish zinc-finger transcription factor gene tsh1. *Gene Expr. Patterns* 7, 318-322 (2007).

31. Nornes, S., Tucker, B. & Lardelli, M. Zebrafish aplnra functions in epiboly. *BMC Res. Notes* 2, 231 (2009).
32. Julich, D., Geisler, R. & Holley, S.A. Integrinalpha5 and delta/notch signaling have complementary spatiotemporal requirements during zebrafish somitogenesis. *Dev. Cell* 8, 575-586 (2005).
33. Gillhouse, M., Wagner Nyholm, M., Hikasa, H., Sokol, S.Y. & Grinblat, Y. Two Frodo/Dapper homologs are expressed in the developing brain and mesoderm of zebrafish. *Dev. Dyn.* 230, 403-409 (2004).
34. Zeng, X.X., Wilm, T.P., Sepich, D.S. & Solnica-Krezel, L. Apelin and its receptor control heart field formation during zebrafish gastrulation. *Dev. Cell* 12, 391-402 (2007).
35. Kobayashi, M., Osanai, H., Kawakami, K. & Yamamoto, M. Expression of three zebrafish Six4 genes in the cranial sensory placodes and the developing somites. *Mech. Dev.* 98, 151-155 (2000).
36. Oates, A.C. & Ho, R.K. Hairy/E(spl)-related (Her) genes are central components of the segmentation oscillator and display redundancy with the Delta/Notch signaling pathway in the formation of anterior segmental boundaries in the zebrafish. *Development* 129, 2929-2946 (2002).
37. Nikaido, M., Law, E.W. & Kelsh, R.N. A systematic survey of expression and function of zebrafish frizzled genes. *PLoS One* 8, e54833 (2013).
38. Fodor, E. *et al.* Full transcriptome analysis of early dorsoventral patterning in zebrafish. *PLoS One* 8, e70053 (2013).
39. Currie, P.D. & Ingham, P.W. Induction of a specific muscle cell type by a hedgehog-like protein in zebrafish. *Nature* 382, 452-455 (1996).

40. Amores, A. *et al.* Zebrafish hox clusters and vertebrate genome evolution. *Science* 282, 1711-1714 (1998).
41. Kim, G.Y. *et al.* HtrA1 is a novel antagonist controlling fibroblast growth factor (FGF) signaling via cleavage of FGF8. *Mol. Cell. Biol.* 32, 4482-4492 (2012).
42. Kai, M., Heisenberg, C.P. & Tada, M. Sphingosine-1-phosphate receptors regulate individual cell behaviours underlying the directed migration of prechordal plate progenitor cells during zebrafish gastrulation. *Development* 135, 3043-3051 (2008).
43. Srinivas, B.P., Woo, J., Leong, W.Y. & Roy, S. A conserved molecular pathway mediates myoblast fusion in insects and vertebrates. *Nat. Genet.* 39, 781-786 (2007).
44. Lukowski, C.M., Ritzel, R.G. & Waskiewicz, A.J. Expression of two insm1-like genes in the developing zebrafish nervous system. *Gene Expr. Patterns* 6, 711-718 (2006).
45. Choe, S.K., Zhang, X., Hirsch, N., Straubhaar, J. & Sagerstrom, C.G. A screen for hoxb1-regulated genes identifies ppp1r14al as a regulator of the rhombomere 4 Fgf-signaling center. *Dev. Biol.* 358, 356-367 (2011).
46. Yu, X., Ng, C.P., Habacher, H. & Roy, S. Foxj1 transcription factors are master regulators of the motile ciliogenic program. *Nat. Genet.* 40, 1445-1453 (2008).
47. Qian, M. *et al.* ENC1-like integrates the retinoic acid/FGF signaling pathways to modulate ciliogenesis of Kupffer's Vesicle during zebrafish embryonic development. *Dev. Biol.* 374, 85-95 (2013).
48. Emoto, Y., Wada, H., Okamoto, H., Kudo, A. & Imai, Y. Retinoic acid-metabolizing enzyme Cyp26a1 is essential for determining territories of hindbrain and spinal cord in zebrafish. *Dev. Biol.* 278, 415-427 (2005).

49. Winkler, C., Schafer, M., Duschl, J., Schartl, M. & Volff, J.N. Functional divergence of two zebrafish midkine growth factors following fish-specific gene duplication. *Genome Res.* 13, 1067-1081 (2003).
50. Rohrschneider, M.R., Elsen, G.E. & Prince, V.E. Zebrafish Hoxb1a regulates multiple downstream genes including prickle1b. *Dev. Biol.* 309, 358-372 (2007).
51. Reifers, F. *et al.* Fgf8 is mutated in zebrafish acerebellar (ace) mutants and is required for maintenance of midbrain-hindbrain boundary development and somitogenesis. *Development* 125, 2381-2395 (1998).
52. Warga, R.M., Mueller, R.L., Ho, R.K. & Kane, D.A. Zebrafish Tbx16 regulates intermediate mesoderm cell fate by attenuating Fgf activity. *Dev. Biol.* 383, 75-89 (2013).